https://doi.org/10.5194/egusphere-2022-197
Preprint. Discussion started: 4 May 2022

Impact of an acceleration of ice sheet melting on monsoon systems

Alizée Chemison[1], Dimitri Defrance[2], Gilles Ramstein[1], and Cyril Caminade[3]

[1]Laboratoire des Sciences du Climat et de l'Environnement (LSCE), CEA, Gif-sur-Yvette, France
[2]The Climate Data factory, Paris, France
[3]Abdus Salam International Centre for Theoretical Physics (ICTP), Earth System Physics Department, Trieste, Italy

Correspondence: Alizée Chemison (alizee.chemison@lsce.ipsl.fr)

Abstract. The study of past climates demonstrated the occurrence of Heinrich events during which major ice discharges occurred at the polar ice sheet, leading to significant additional sea level rise. Heinrich events strongly influenced the oceanic circulation and global climate. However, standard climate change scenarios (Representative Concentration Pathways or RCPs) do not consider such potential rapid ice-sheet collapse; RCPs only consider the dynamics evolution of greenhouse gases emissions. We carried out water-hosing simulations using the Institute Pierre Simon Laplace global Climate Model (IPSL-CM5A) to simulate a rapid melting of the Greenland and Antarctic ice-sheets, equivalent to +1 and +3 m additional sea level rise (SLR). Freshwater inputs were added to the standard RCP8.5 emission scenario over the 21^{st} century. The contribution to the SLR from Greenland or from Antarctic ice sheets have differentiated impacts. The fresh water input in the Antarctic is diluted by the circumpolar current and its global impact is moderate. Conversely, a rapid melting of the ice-sheet in the North Atlantic slows down the Atlantic meridional overturning circulation. This slowdown leads to changes in winds, inter-hemispheric temperature and pressure gradients, resulting in a southward shift of the tropical rain belt over the Atlantic and Eastern Pacific region. The American and African monsoons are strongly affected and shift to the south. The North American monsoon occurs later, while the South American monsoon starts earlier. The North African monsoon is drier during boreal summer while the South African monsoon intensifies during austral summer. Simulated changes were not significant for the Asian and Australian monsoons.

1 Introduction

Monsoons influence all tropical regions, providing the vast majority of rainfall in one season. Consequently, monsoons have a significant impact on two thirds of the world's population. Tropical monsoons have a large inter-annual to multi-decadal variability that modulate drought, flooding and other climatic extremes that have strong impacts on human societies, agriculture and economy. Monsoons are related to atmospheric moisture content, land–sea temperature contrast (Zhou and Zou, 2010), land cover and use (Timbal and Arblaster, 2006), atmospheric aerosol loadings (Lau et al., 2008). Climate change is expected to significantly alter monsoon systems (Zhisheng et al., 2015). Studying the future evolution of monsoons is essential to guide adaptation measures. Climate change impact on tropical monsoons has been extensively studied using coupled Global Climate Models (GCMs) that provide predictions of future climate under various greenhouse gases (GHGs) emission scenarios. The Coupled Model Intercomparison Project 5 (CMIP5) aimed to coordinate climate simulations produced by different international research groups. CMIP5 has used the Representative Concentration Pathways (RCPs) scenarios (Meehl et al., 2000),

https://doi.org/10.5194/egusphere-2022-197
Preprint. Discussion started: 4 May 2022

which are GHGs emission pathways in CO_2 equivalent, corresponding to different radiative forcing scenarios at the end of the 21^{st} century (Moss et al., 2010; Taylor et al., 2012). From these scenarios, it has been shown that monsoons are significantly affected by climate change (Wang et al., 2021).

It is difficult to estimate the evolution of the global monsoon in the short term (2020-2040) because the uncertainty and internal variability across GCMs are more important than the signal itself (Lee et al., 2021). Nevertheless, precipitation is expected to increase by 1 to 3 % per 1 °C increase during the mid (2041-2060) and long term (2081-2100), see Lee et al. (2021). The global monsoon area, total precipitation and precipitation intensity are simulated to increase by most CMIP5 models at the end of the 21^{st} century (Hsu et al., 2013; Kitoh et al., 2013). These increases are linked to an increase in evaporation, and therefore to an increase in atmospheric moisture flow, but also to increased temperature contrast between the continents and the oceans. Continents are warming up faster than the oceans in the context of global warming. Moreover, Lee and Wang (2014) show a zonal asymmetry between the eastern monsoons, with increased precipitation, and the western monsoons, with decreased precipitation. They also show an asymmetry between the northern and southern hemispheres. The northern hemisphere will receive more rainfall in the future while the southern hemisphere will receive less. In the northern hemisphere the monsoon period lasts longer with an earlier start and later cessation date (Lee and Wang, 2014). Extreme precipitation events as well as days of drought conditions are also simulated to increase in future (Shongwe et al., 2011; Cavazos et al., 2008).

At regional scale, monsoons are differently affected by climate change. CMIP3 and CMIP5 models show a rainfall increase across the Asian monsoons (Turner and Annamalai, 2012; Li et al., 2015). These changes are considered with medium confidence in the latest IPCC report (Ranasinghe et al., 2021). The East Asian monsoon (EAS) and the Southern Asian monsoon (Indian monsoon) are intensifying with increasing mean and extreme rainfall (Jiang et al., 2012). An increase in heavy precipitation events and a longer season for EAS was highlighted by Suhaila et al. (2010).

For the Maritime continent region (between Asia and Australia) and Australia, the multi-model agreement for future rainfall changes is low (Christensen et al., 2013). Even at higher spatial resolution (50 km), current state of the art GCMs are not suited to capture the fine scale climatic processes occurring in this region (Turner and Annamalai, 2012). Accurate GCM simulation over the Maritime continent depends on their ability to reproduce the El Niño Southern Oscillation (ENSO) signal in the Warm Pool region (Turner and Annamalai, 2012). Jourdain et al. (2013) show an increase in Australian rainfall using RCP8.5 at the end of the 21^{st} century. However, these simulated changes are small and have substantial uncertainties (Ranasinghe et al., 2021).

For the Americas, two monsoon systems are commonly identified (Christensen et al., 2013): the North American Monsoon System (NAMS) and the South American Monsoon System (SAMS). For the NAMS, a decrease in precipitation is simulated over the 21^{st} century, although significant differences are shown across GCMs. However, there is a robust increase in temperature, in the number of dry days and extreme events simulated over this region at the end of the 21^{st} century (Duffy and Tebaldi,

https://doi.org/10.5194/egusphere-2022-197
Preprint. Discussion started: 4 May 2022

2012). In addition, Cook and Seager (2013) show that changes in total rainfall are small and with low confidence. A shift in the NAMS monsoon season is also simulated, with a decrease in rainfall at the beginning of the season (June-July) and an increase towards the end (September-October). For the SAMS, there is a seasonal amplification with an earlier start and later cessation date (Jones and Carvalho, 2013). Jones and Carvalho (2013) show an increase in precipitation over Brazil, Uruguay and northern Argentina. The fifth IPCC report indicates medium confidence that precipitation will remain unchanged in this region (Christensen et al., 2013).

A rainfall intensity increase is simulated over western, central and southern Africa with however less rainy days simulated over the western and southern African regions (Dunning et al., 2018). Over eastern Africa, two rainy seasons occur: the so-called short rains from October to December and long rains from March to May. A significant increase in future rainfall during the long rainy season is usually simulated over East Africa. For the West African monsoon, there are large rainfall differences simulated across GCMs (Monerie et al., 2020). However, simulated trends for CMIP3 and CMIP5 are similar with a slight increase in precipitation linked to a delayed shutdown of the monsoon (Biasutti and Sobel, 2009; Christensen et al., 2013). Dunning et al. (2018) show a later onset of the monsoon season with a northward shift of the rainbelt between August and December. The study of (Biasutti and Sobel, 2009), based on CMIP3 models, projects a shorter rainy season with a late start of the semi-arid African Sahel. An extension of the dry season is simulated over the southern part of Africa (Mariotti et al., 2014).

The study of palaeoclimatology with GCMs has shown the ability of models to simulate strong changes in precipitation at longer time scales. For example, the simulation of the green Sahara during the middle Holocene has always been challenging, with climate models usually underestimating the northward extension of the African monsoon. Nevertheless, the inclusion of new processes and boundary condition including lakes (Krinner et al., 2012) or aerosols (Thompson et al., 2019) allowed simulations to reproduce the greening of the Sahara during the early to mid-Holocene (Krinner et al., 2012). Climate observations and future climate scenarios both indicate that global warming is occurring and the warming is more pronounced at high latitudes. This warming at the poles leads to an increase in ice sheet melting (Peterson et al., 2006). This melting releases a significant volume of fresh water which contributes to additional Sea Level Rise (SLR) (Rignot et al., 2011).

Melting is a non-linear process due to positive feedbacks associated with temperature increase (Fettweis et al., 2012). The melting of the ice sheet decreases surface albedo, consequently the surface absorbs more solar energy leading to additional ice sheet melting. In addition rising temperature can lead to increased liquid with respect to solid precipitation at high latitudes, which can increase the ice sheet mass loss. This mechanism occurs for the Greenland ice sheet (Fettweis et al., 2012), unlike Antarctica, where an increase in solid precipitation makes the mass balance more complicated to predict (Rignot et al., 2011). Finally, a fraction of mass loss is in relation with the glacier dynamics (Rignot et al., 2011; Fettweis et al., 2012). Observations suggest important processes responsible for glacier front destabilization that are not included in current state of the art dynamical ice sheet models, such as the role of ice discharge on the total Greenland ice-sheet mass balance (Gillet-Chaulet

https://doi.org/10.5194/egusphere-2022-197
Preprint. Discussion started: 4 May 2022

et al., 2012). Such destabilization could lead to an iceberg break-up which, in some ways, might be similar to past Heinrich events (Broecker et al., 1992). It is noteworthy that deglaciation occurred over several thousand years when CO_2 concentration only varied from 180 ppm (glacial period) to 280 ppm (interglacial period). Recent historical CO_2 emissions ranged from 280 to 415 ppm and they might reach 500 ppm or more by the end of the 21^{st} century. In addition, the last deglaciation occurring during the first half of the Holocene was strongly non-linear with an accelerated phase of melting (Mimura, 2013). Therefore, it is important to estimate the impact of such accelerated phases associated with Greenland and Antarctica melting (Hemming, 2004). The SLR predicted at the end of the 21^{st} century by the IPCC fifth Assessment Report (AR5) is ranging between 0.52 and 0.98 m (Church et al., 2013). Nevertheless, non-linear climatic processes may occur, as for instance DeConto and Pollard (2016) have shown: a rapid ice sheet destabilization could lead to an additional SLR well exceeding 1 m.

GCMs are often not fully coupled with ice sheet models. Even if some GCMs include melting ice (Church et al., 2013), studies have shown that the melting predicted by these models is underestimated (Rignot et al., 2011; Gillet-Chaulet et al., 2012). Estimates of additional SLR are not directly available from GCMs outputs. Ice sheet models or regional models forced by temperature and rainfall simulated by GCMs are used to estimate additional SLR off-line. (Fettweis et al., 2012). However, the addition of fresh water due to the melting of the ice sheet at high latitudes is having a global impact on the climate (Mimura, 2013).

A major release of fresh water, linked to a tipping point of the ice sheet, would not be without consequences. In Greenland, the inputs of fresh-water slow down the Atlantic Meridional Overturning Circulation (AMOC) (Bakker et al., 2016). A release of fresh water in the North Atlantic leads to a cooling of the Northern Hemisphere and a southward shift of the inter-tropical convergence zone (ITCZ) in the Atlantic (Schiller et al., 1997; Vellinga and Wood, 2002; Jackson et al., 2015). This finding is consistent at different time scales: for paleo modelling studies (Kageyama et al., 2013; Marzin et al., 2013a), for pre-industrial historical simulations (Vellinga and Wood, 2002; Stouffer et al., 2006) or for future climate simulations considering an increase in GHGs emissions (Vellinga and Wood, 2008; Liu et al., 2020). Consequently, a slowdown of the AMOC will have global consequences and this is clearly demonstrated in paleoclimatology during Heinrich events; it is possible to find proxy of induced changed in temperature and precipitation in many places on earth (Clement and Peterson, 2008). Simulations of such a rapid melting have impacts on the Asian monsoon (Marzin et al., 2013b), the African monsoon (Mulitza et al., 2008; Marzin et al., 2013a) and might induce changes in European and American temperature and precipitation (Jackson et al., 2015). These feedbacks and the magnitude of temperature and precipitation changes outside the North Atlantic region depend on the mean simulated climate (Swingedouw et al., 2009b). Although GCMs have biases, the consequences of an influx of fresh water into the North Atlantic, a cooling of the North Atlantic and a southward shift of tropical precipitation, has been shown in simulations conducted with different GCMs (Stouffer et al., 2006; Swingedouw et al., 2013). The melting of Antarctica can moderate the simulated rise in temperature in the southern hemisphere (Swingedouw et al., 2008). Competition between the deep-waters formed in the North Atlantic (NA) and the Southern Ocean (SO) leads to a process called the bipolar oceanic seesaw (Stocker, 1998). Swingedouw et al. (2009a) show that the release of freshwater in the Southern Hemisphere, linked to the melting of the Antarctic, can impact NA Deep-Water (NADW). This effect occurs because of three processes, the deep-water adjustment

https://doi.org/10.5194/egusphere-2022-197
Preprint. Discussion started: 4 May 2022

which strengthens the NADW cell, the SO salinity anomaly which weakens the NADW cell and the increase in wind stress in the Southern Hemisphere which strengthens the NADW cell. These processes act on different time scales ranging from a few to thirty years (Swingedouw et al., 2009a).

To determine the impact of a significant release of fresh water at high/low latitudes on tropical monsoons, we used a simulation framework developed by Defrance et al. (2017). A release of freshwater is simulated in the North Atlantic (offshore Antarctica) to simulate a partial melting of the Greenland (West Antarctica) ice-sheet. This freshwater release is added to the standard RCP8.5 scenario to simulate a break-up of the ice sheet using the Institute Pierre Simon Laplace Climate Model, version 5A (IPSL-CM5A).

This study aims to understand the impact of a rapid ice-sheet melting on monsoons and the physical mechanisms at play. First, we focus on the impact of ice sheet melting on oceanic and atmospheric circulation (Sect. 3.1 and Sect.3.2 respectively). In a second step, we will study more detailed impacts of such melting on monsoons, first globally and then regionally (Sect. 3.3 and Sect. 3.4 respectively). Finally, we will discuss these results and will provide final recommendations (Sect. 4).

2 Methods

2.1 Climate model

All experiments were conducted using the IPSL-CM5A model at Low spatial Resolution (IPSL-CM5A-LR, 3.75 °in longitude and 1.875 °in latitude), described by Dufresne et al. (2013). IPSL-CM5A is one of the global climate model used for CMIP5 (Taylor et al., 2012), that feeds into the IPCC 5th assessment report. This model is a atmosphere ocean global climate model (AOGCM). This GCM includes an atmosphere-land surface model coupled to an ocean-sea ice model. This model is made up of physical and biogeochemistry models (Dufresne et al., 2013). The dynamical atmospheric model is LMDz (Laboratoire de Météorologie Dynamique zoom) version 5A with 39 vertical levels, 15 levels of them are below 20 km (Hourdin et al., 2013). The ORCHIDEE (ORganizing Carbon and Hydrology In Dynamic EcosystEms) land surface model is included in IPSL-CM5A-LR (Krinner et al., 2005). NEMOv3.2 (for Nucleus for European Modelling of Ocean) is the ocean model included in IPSL-CM5A (Madec et al., 2017). NEMOv3.2 inludes the simulation of ocean dynamics with OPA (Océan PArallélisé), of biogeochemistry processes with PISCES (Pelagic Interaction Scheme for Carbon and Ecosystem Studies) (Aumont and Bopp, 2006) and sea ice processes with LIM2 (Louvain-la-Neuve Sea Ice Model, Version 2) (Fichefet and Maqueda, 1997). The OAsis (Ocean Atmosphere Sea Ice Soil) coupler allows the synchronization of all models and the exchange of energy and moisture fluxes between the different sub-climatic systems (Valcke, 2013). The biogeochemistry models are INCA (The INteraction with Chemistry and Aerosol) for tropospheric chemistry and aerosols (Hauglustaine et al., 2004), the REPROBUS (Reactive Processes Ruling the Ozone Budget in the Stratosphere) module for stratospheric chemistry (Lefevre et al., 1994). The prescribed variables are CO_2 and other greenhouse gases emissions based on RCP scenarios (Moss et al., 2010), land use

https://doi.org/10.5194/egusphere-2022-197
Preprint. Discussion started: 4 May 2022

(Hurtt et al., 2011), solar irradiance (Lean et al., 2005), and volcanic aerosols (Dufresne et al., 2013).

2.2 Experimental design

The experimental design used in this study (Chemison et al., 2022) is based on Defrance et al. (2017). The RCP8.5 scenario (Moss et al., 2010) is used as our reference simulation. RCP8.5 is a worst-case scenario assuming the continuation of recent trends without mitigation during the 21st century and leading to an atmospheric radiative imbalance of 8.5 W.m^{-2} by 2100 (Moss et al., 2010). To simulate the ice-sheet melting, two sets of simulations were used. The first one corresponds to a partial melting of the Greenland Ice-Sheet (GrIS scenarios) and the second one to a melting of the West Antarctica Ice Sheet (WAIS scenarios). Freshwater fluxes (FWFs) of 0.22 and 0.68 Sv (where 1 Sv = 10^6 m^{3}s^{-1}) for the GrIS scenarios, and 0.68 Sv for the WAIS scenario, were introduced from 2020 to 2070 using the common RCP8.5 radiative forcing scenario, leading to +1 and +3 m additional SLR respectively. These simulations are hereafter referred as to GrIS1m, GrIS3m and WAIS3m. For the GrIS scenarios, the fresh water is added in the Labrador Sea (45 °N–65 °N, 45 °W–5 °E) where deep water is formed. For WAIS3m, fresh water is added into the western Antarctic Ocean, off the coasts of Southern America (Defrance et al., 2020). The choice to introduce large amounts of freswater aims to magnify potential impacts of rapid ice sheet melting on monsoon systems, despite known low sensitivity of current climate models to the amount of freshwater release (Swingedouw et al., 2013; Hansen et al., 2016).

We compare a mid-century period (2041-2070) during freshwater release, with the historical period (1976-2005) for both GrIS and WAIS scenarios. To quantify the potential impact of melting ice sheet on ocean circulation, we study the evolution of the AMOC, which is derived from the maximum annual mean stream function at 30 °N based on the criterion by Cheng et al. (2013).

2.3 The monsoon domains

Monsoon areas are defined based on the criterion by Lee and Wang (2014). A monsoon area is characterised by an annual difference in precipitation between local summer and winter exceeding a threshold of 2.5 mm day^{-1} and the summer precipitation must exceed 55 % of the annual total. To compare observed and simulated monsoon areas, observed rainfall data is based on the Global Precipitation Climatology Project (GPCP), Monthly V2.3 available from the NOAA PSL, Boulder, Colorado, USA (Adler et al., 2018). This data was averaged between 1979 and 2005 and compared with the historical simulation from 1976 to 2005.

Each regional monsoon was defined following fifth IPCC report naming convention (Figure 14.3 in Christensen et al. (2013)): the North America Monsoon System (NAMS), South America Monsoon System (SAMS), North Africa (NAF), Southern Africa (SAF), Eastern Asia (EAS), South Asia (SAS) and Australia and Maritime Continent (AUSMC), see Table 1 and Fig. 1. The equator separates the northern hemisphere monsoons whose summer wet season lasts from May until September (MJJAS),

https://doi.org/10.5194/egusphere-2022-197
Preprint. Discussion started: 4 May 2022

Table 1. List of regions and the associated monsoon period. Only land grid points are used in the analysis. See figure 1 for the graphical representation of regions.

Monsoon Acronym	Name	Domain	Period of monsoon
NAMS	North America Monsoon System	1°N-39°N, 109°W-53°W	MJJAS
SAMS	South America Monsoon System	1°S-29°S, 79°W-38°W	NDJFM
NAF	North Africa	1°N-12°N, 11°W-38°E	MJJAS
SAF	Southern Africa	1°S-31°S, 15°E-49°E	NDJFM
EAS	Eastern Asia	22°N-39°N, 101°E-128°E	MJJAS
SAS	South Asia	1°N-31°N, 75°E-128°E	MJJAS
AUSMC	Australia and Maritime Continent	1°S–20S°, 101°E–150°E	NDJFM

and the southern hemisphere monsoons where the summer period lasts from November to March (NDJFM) following Wang and Ding (2008), Wang et al. (2011) and Lee and Wang (2014).

Monsoon areas consist of any grid point corresponding, in at least one of the simulations, to the aforementioned criterion (Lee and Wang, 2014). Thus, the selected monsoon areas include both the historical monsoon region and the monsoon regions for all simulations (RCP8.5, GrIS1m, GrIS3m, WAIS3m). All grid points per monsoon region were retained to derive spatial averages, except for the AUSMC box for which one outlier (southernmost point) was removed. Land only data was considered. Hovmöller diagrams were derived for each monsoon region and rainfall was averaged longitudinally. They represent the average monthly precipitation over our 30-year study period. Then, the difference between the future period (2041-2070) and the historical period (1976-2005) were calculated. The statistical significance of this difference was evaluated using the Wilcoxon-Mann-Whitney test for p-values greater than 0.05 (Seneviratne et al., 2013).

Hovmöller diagrams are shown for NAMS, SAMS, NAF, SAF and SAS. Diagrams for AUSMC and EAS are presented in Appendix A2. It is noteworthy that changes for AUSMC and EAS are mostly non-significant and there are too few land pixels for the AUSMC region.

2.4 Characterisation of monsoons

Six indices, defined by the Expert Team on Climate Change Detection and Indices (ETCCDI), were used to determine changes in daily rainfall extremes and statistics per monsoon region (Sillmann et al., 2013): the average precipitation (Pav), the number of rainy days (R1mm), simple precipitation daily intensity index (SDII), seasonal maximum 5 days precipitation total (RX5day), seasonal maximum consecutive dry days (CDD) and seasonal maximum consecutive wet days (CWD). The indices are calculated annually for the May to September period over the Northern Hemisphere and for the November to March period for the Southern Hemisphere. Calculation details for each index are provided in Table 2.

https://doi.org/10.5194/egusphere-2022-197
Preprint. Discussion started: 4 May 2022

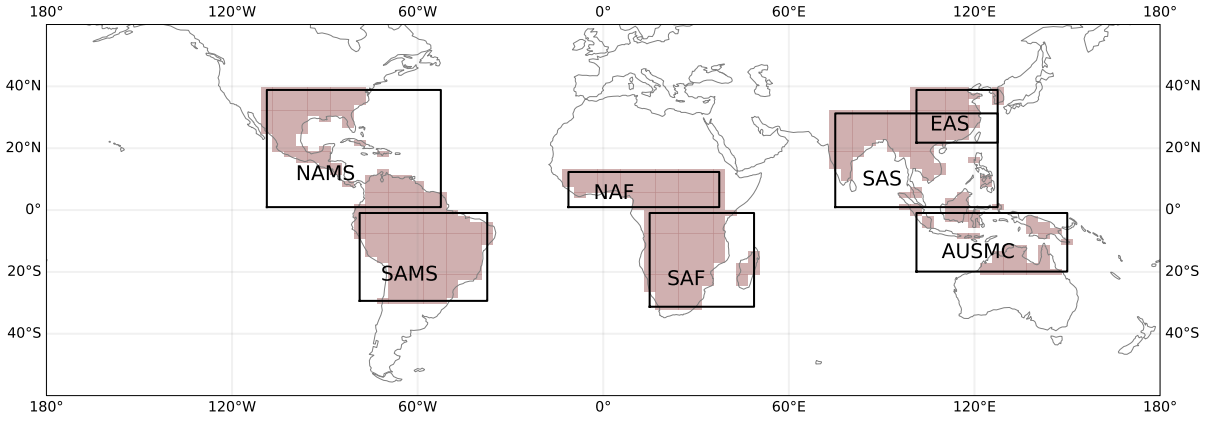

Figure 1. Regions used in this study. See Table 1 and methods for more details.

The validation of these indicators for our simulations is presented in supplementary materials by comparing the inter-annual variability of each index for each monsoon between the historical simulation and the EartH2Observe, WFDEI and ERA-Interim data Merged and Bias-corrected data for ISIMIP (EWEMBI) (Lange, 2016). To study the impact of each simulation on these monsoon indices, the difference in inter-annual variability for each simulation between the period 2041-2070 and the historical simulation 1976-2005 is then calculated as the difference between a year and the historical mean divided by the historical mean and converted to a percentage: $100.(year_i - mean_{hist})/mean_{hist}$ These results are presented in the form of whisker boxes for each region and each simulation.

https://doi.org/10.5194/egusphere-2022-197
Preprint. Discussion started: 4 May 2022

Table 2. Definition and description of the monsoon indices used in this study.

Label	Index name	Index definition	Units
Pav	Total wet-day precipitation	Let PRij be the daily precipitation amount on day i in period j. If I represents the number of days in j, then: $Pavj = \sum_{n=1}^{i} PRij$	mm
R1mm	Annual count of wet days	Let PRij be the daily precipitation amount on day i in period j. Count the number of days where PRij > 1 mm	days
SDII	Simple precipitation intensity index	Let PRwj be the daily precipitation amount on wet days, PR >= 1 mm in period j. If W represents number of wet days in j, then: $SDIIj = (\sum_{w=1}^{w} PRwj)W^{-1}$	mm day^{-1}
RX5day	Maximum consecutive 5-day precipitation	Let PRkj be the precipitation amount for the 5 days interval ending k, period j. Then maximum 5 days values for period j are: $RX5dayj = max(PRkj)$	mm
CDD	Maximum length of dry spell, maximum number of consecutive days with RR < 1 mm	Let PRij be the daily precipitation amount on day i in period j. Count the largest number of consecutive days where PRij < 1 mm	days
CWD	Maximum length of wet spell, maximum number of consecutive days with RR $\geq$ 1 mm	Let PRij be the daily precipitation amount on day i in period j. Count the largest number of consecutive days where PRij > 1 mm	days

3 Results

3.1 Ocean Dynamics

The most direct impact of the addition of fresh water, resulting from an ice melting, occurs in the ocean. Future changes for the RCP8.5 simulation correspond to a -4 Sv decrease of the stream function between 500 and 2500 m depth in the North Atlantic (Fig. 2a). This difference is slightly reduced for the WAIS3m scenario (Fig. 2b) denoting a moderate impact of Antarctica ice melting on the North Atlantic Ocean circulation. This moderate impact may be related to the presence of the circumpolar current around the Antarctica continent which tends to dilute the FWF disturbance. Conversely, the addition of FWF in the North Atlantic associated with the melting of the Greenland ice sheet strongly amplifies the simulated decrease in stream function

https://doi.org/10.5194/egusphere-2022-197
Preprint. Discussion started: 4 May 2022

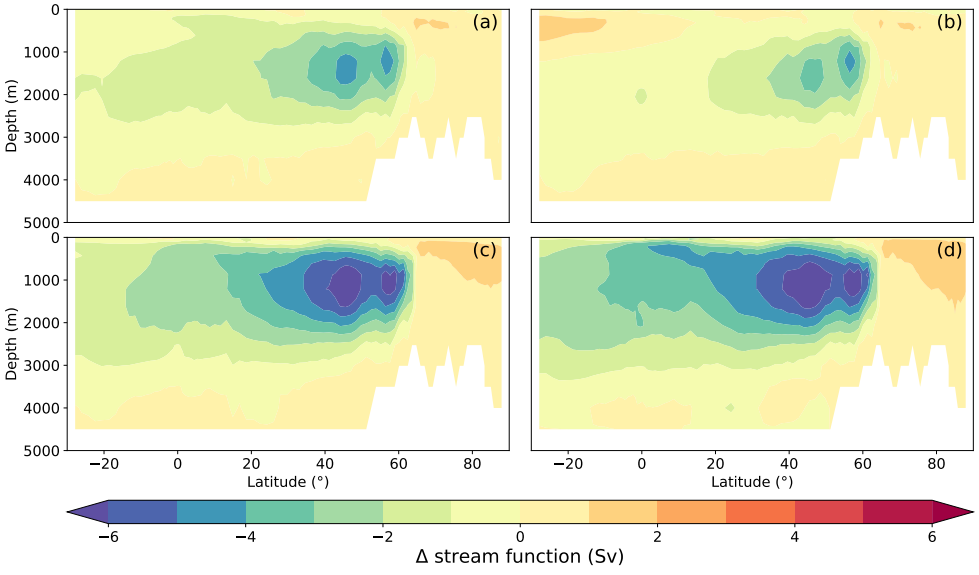

Figure 2. Stream function difference between future scenarios (2041-2070) and historical simulation (1976-2005). The future scenarios are a) RCP8.5, b) WAIS3m, c) GrIS1m and d) GrIS3m.

(about -6 Sv between 500-2500 m). The larger the amount of freshwater added, the greater the decrease in simulated oceanic stream function (Fig. 2c and Fig. 2d). The addition of fresh water in the Labrador Sea changes the water density resulting in changes in oceanic currents. The seasonal signal is weak although there are slightly stronger differences simulated in boreal summer with respect to winter for the GrIS scenarios (see Appendix A Figure A1 and Figure A2).

These results are consistent with the simulated evolution of the AMOC during the 21^{st} century (Fig. 3). In 2020, before the simulated release of freshwater, all simulations are extremely similar. Simulated AMOC ranges between 7 and 8 Sv, and small differences across simulations might be related to internal model variability (Fig. 3). Between 2025 and 2050, the AMOC simulated for the RCP8.5 scenario decreases to 6 Sv and then increases to 8 Sv while the AMOC for the WAIS3m scenario remains relatively constant. After 2050, the AMOC slowly decreases to 4 Sv for WAIS3m and 5 Sv for RCP8.5. The AMOC simulated for the scenarios with the melting of the Greenland ice sheet, GrIS1m and GrIS3m, shows larger changes. For GrIS1m and GrIS3m, the AMOC decreases to 4 Sv between 2025 and 2030, then to 2 Sv between 2040 and 2050, with a 1 Sv minimum reached between 2060 and 2070. From 2070 onwards, freshwater release stops in our experiments, the AMOC simulated by GrIS1m and GrIS3m then stabilises and oscillates at values of about 2 Sv. The release of fresh water in Antarctica (WAIS3m) initially buffers the simulated slowdown of the AMOC in the RCP8.5 experiment (Fig. 3). Freshwater input in the North Atlantic breaks down the AMOC, with an almost complete collapse simulated by 2060-2070 (Fig. 3). The amount of released freshwater in the North Atlantic has a limited impact on AMOC changes, as values for the GrIS1m and GrIS3m scenarios are relatively similar for the 21^{st} century (Fig. 3).

https://doi.org/10.5194/egusphere-2022-197
Preprint. Discussion started: 4 May 2022

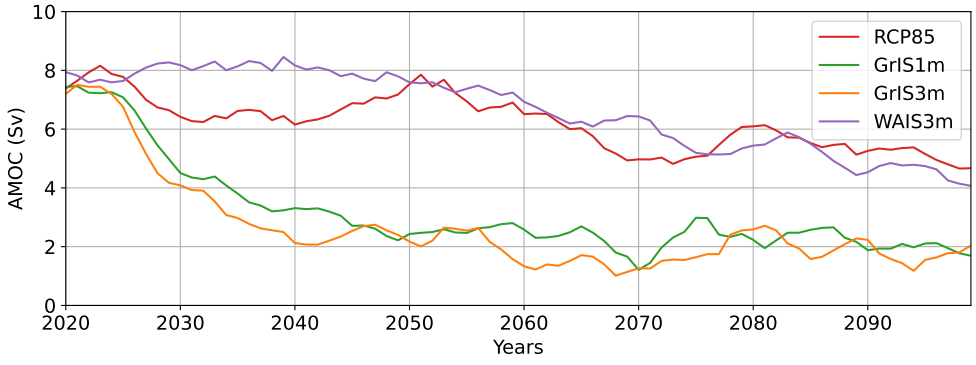

Figure 3. Simulated AMOC between 2020 and 2099 for different scenarios: RCP8.5 in red, GrIS1m in green, GrIS3m in orange and WAIS3m in purple. The AMOC index is derived from the maximum annual mean stream function at 30 °N from Cheng et al. (2013)

3.2 Atmosphere Dynamics

Differences between future scenarios and the historical period are shown for several atmospheric variables (temperature, rainfall, sea level pressure and winds at 850hPa) during boreal summer on Figure 4, and austral summer on Figure 5. A large increase in temperature is shown at global scale for the RCP8.5 scenario, with simulated temperature differences of about 10 °C at the North Pole during boreal winter (Fig. 5a). This high latitude increase in temperature is slightly amplified in the WAIS3m scenario (Fig. 5c). Conversely, the effect of the RCP8.5 radiative forcing on temperature is strongly buffered by the melting of the Greenland ice sheet (GrIS1m and GrIS3m). Simulated temperature increases for GrIS1m (Fig. 4e and Fig. 5e) and GrIS3m (Fig. 4g and Fig. 5g) are much smaller all year round. The fresh water released into the Labrador Sea cools down this region; this local cooling extends to the western part of the Northern Atlantic Ocean for GrIS3m (Fig. 4.e, Fig. 5.e). The induced cooling of the North Atlantic is more pronounced during boreal winter (Fig. 5e). For the WAIS3m simulation, the cooling due to the melting of the Western Antarctica is shown during austral summer (Fig. 5c) and is greatly amplified during austral winter (Fig. 4c). WAIS3m shows a regional cooling along the Antarctica coast which is linked to the circumpolar current (Fig. 4c and Fig. 5c).

All simulations show a decrease in sea level pressure (SLP) at both poles in boreal summer and winter (Fig. 4 and Fig. 5). During boreal summer (MJJAS), there is a decrease in SLP over the Northern Hemisphere, no change in simulated rainfall between 10 °N and 30 °S and an increase in SLP in the Southern Hemisphere between 30 °S and 60 °S for the RCP8.5 (Fig. 4b) and WAIS3m (Fig. 4d) simulations. Over the Eastern Pacific and Tropical Atlantic Oceans, the RCP8.5 simulation shows a southward shift of the ITCZ (Fig. 4b). These changes are not simulated in WAIS3m, a slight increase in rainfall is simulated over this region with more westerly winds (Fig. 4d). In the GrIS1m and GrIS3m simulations, SLP increases near the coasts of Central America and over the southern USA during boreal summer (Fig.4f and Fig. 4h). A decrease in SLP is simulated between 30 °S and 60 °S for GrIS1m (Fig. 4f) and GrIS3m (Fig. 4h) during boreal summer. The resulting inter-

https://doi.org/10.5194/egusphere-2022-197
Preprint. Discussion started: 4 May 2022

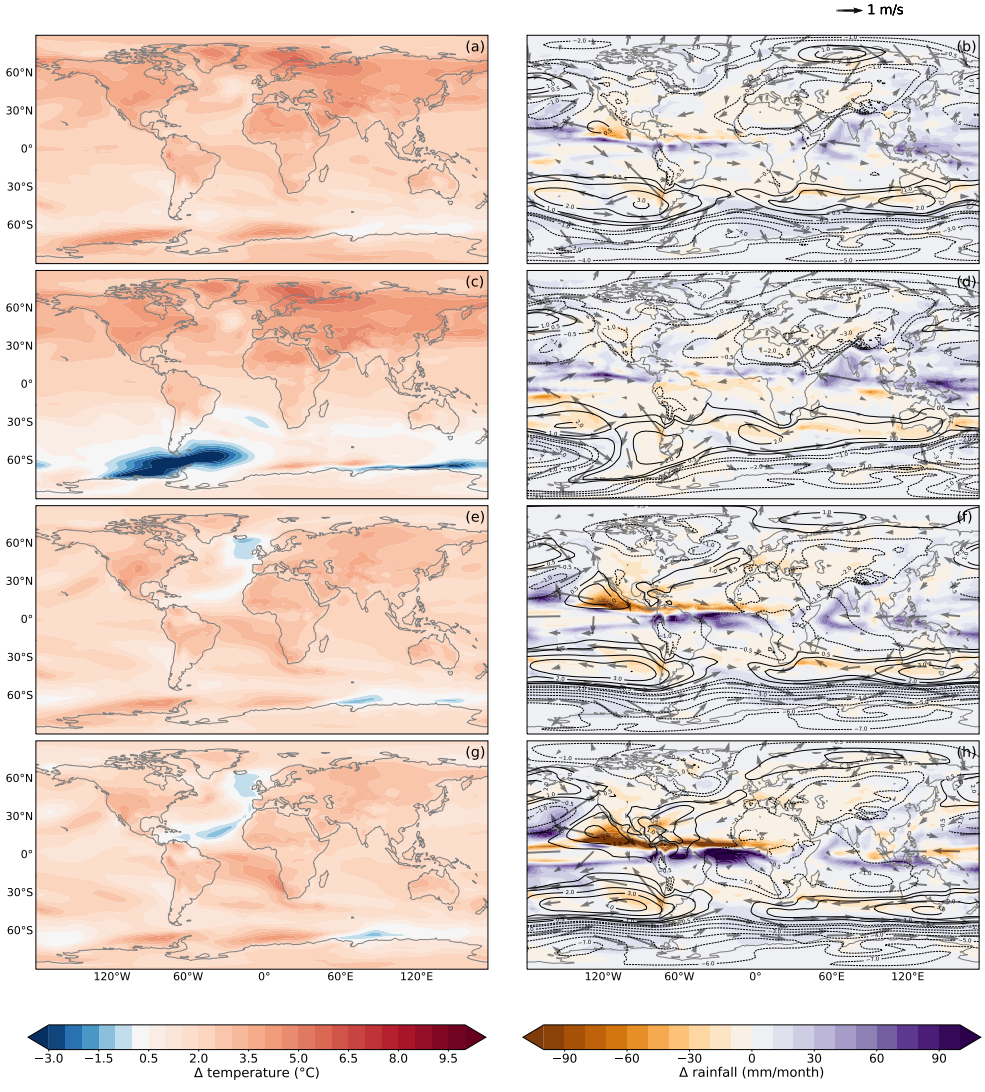

Figure 4. Difference between future scenarios (2041-2070) and historical simulation (1976-2005) for the boreal summer season (MJJAS). Left column depicts the surface temperature difference (a,c,e,g), right column shows the difference in rainfall (shading), in SLP (black contours) and the wind difference at 850hPa (vectors) (b,d,f,h). The futures scenarios are a.b) RCP85, c.d) WAIS3m, e.f) GrIS1m and g.h) GrIS3m.

hemispheric SLP gradient causes a southward shift of the rain belt (Fig. 4f and Fig 4h). The SLP gradient between the southern and northern hemispheres increases with the addition of fresh water in the North Atlantic Ocean. This gradient is consistent with an increased southward pressure force that pushes the ITCZ southward over the Atlantic, leading to a significant decrease (increase) in rainfall north (south) of the Equator. A similar mechanism is highlighted during boreal winter (NDJFM) with an increase in precipitation simulated further south, over Brazil and southern Africa (Fig. 5f and Fig. 5h).

https://doi.org/10.5194/egusphere-2022-197
Preprint. Discussion started: 4 May 2022

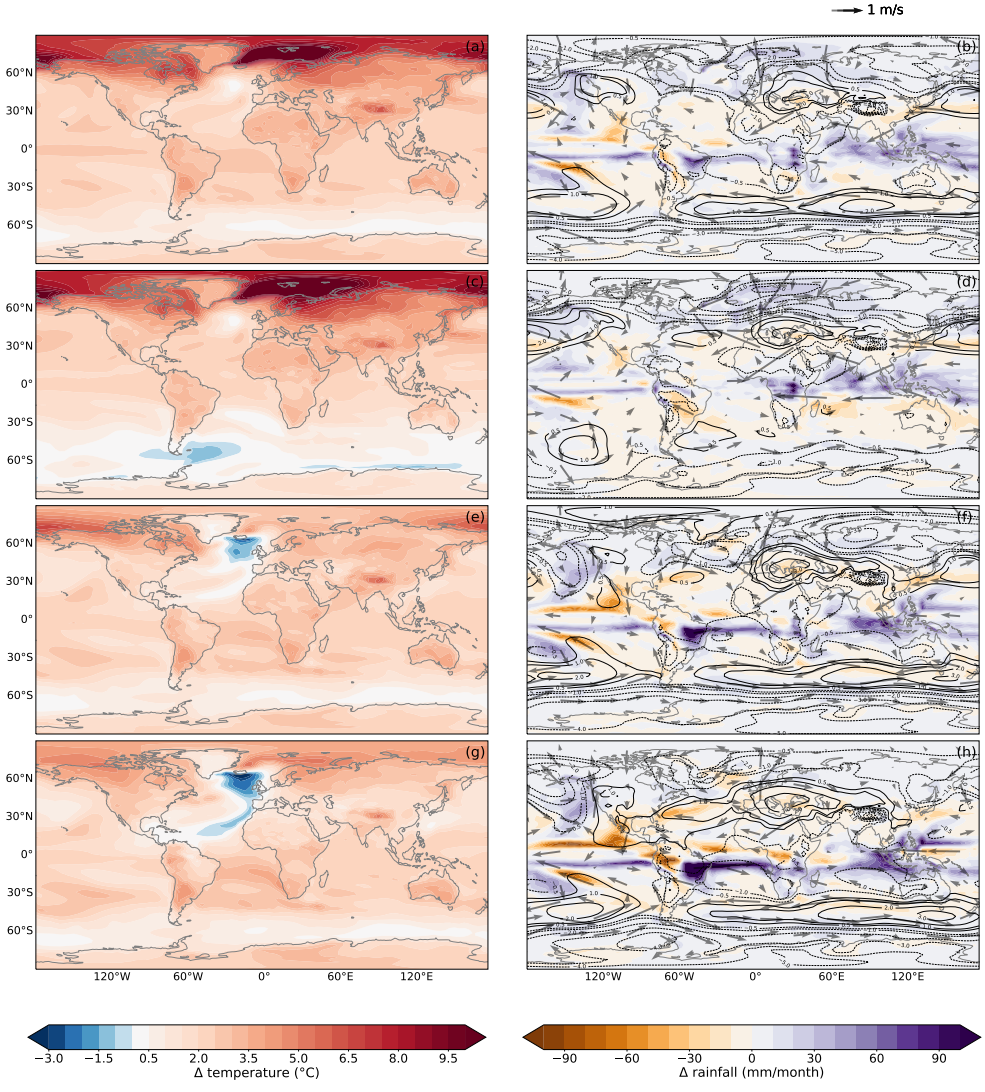

Figure 5. Difference between future scenarios (2041-2070) and historical simulation (1976-2005) for the boreal winter season (NDJFM). Left column depicts the surface temperature difference (a,c,e,g), right column shows the difference in rainfall (shading), in SLP (black contours) and the wind difference at 850hPa (vectors) (b,d,f,h). The futures scenarios are a.b) RCP85, c.d) WAIS3m, e.f) GrIS1m and g.h) GrIS3m.

3.3 Impacts on global monsoon

All model experiments tend to simulate a double Intertropical Convergence Zone (ITCZ), a classical drawback in state of the art GCMs (Fig. 6). Despite this standard bias, the IPSL-CM5 model tends to reproduce the main tropical monsoon areas (shaded areas on Fig. 6) with respect to observed estimates (black contours on Fig. 6). However, the West African and Indian monsoons

https://doi.org/10.5194/egusphere-2022-197
Preprint. Discussion started: 4 May 2022

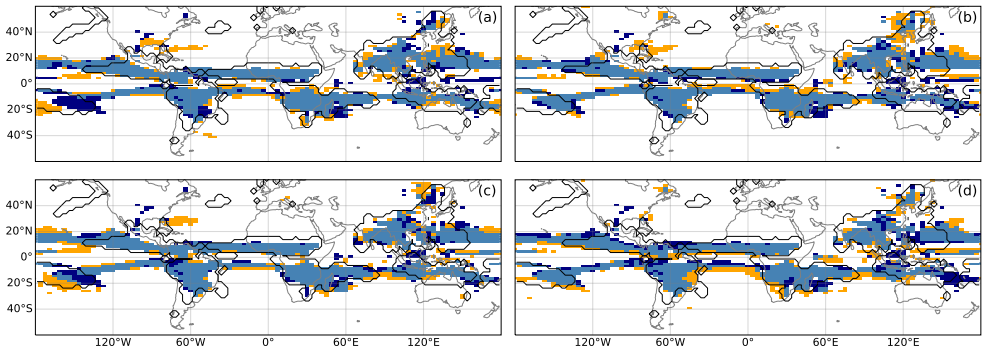

Figure 6. Observed (black contour) and simulated (shading) global monsoon regions, based on the criterion by Lee and Wang (2014) for a) RCP8.5, b) WAIS3m, c) GrIS1m, d) GrIS3m. Orange (dark blue) shading depicts monsoon regions simulated for the historical (future) period. Light blue shading shows the monsoon domains that spatially intersect for both periods.

are simulated too far South and the model also underestimates rainfall over central America and northern Australia (Fig. 6). Over the African continent, simulated future changes are moderate over the Sahel for the RCP8.5 (Fig 6a) and WAIS3m scenario (Fig 6b). A southward shift of the ITCZ is simulated over the Tropical Atlantic region in the GrIS1m (Fig. 6c) and GrIS3m (Fig. 6d) experiments. In GrIS3m, the future rain belt extends further south over southern Africa and south-western Brazil (Fig. 6d). Most experiments tend to suggest that south-eastern US states might become Tropical monsoon regions in future. A northward shift of monsoon regions over northern China is also depicted.

3.4 Impacts on regional monsoons

For the NAMS, rainfall is large from May to September between the equator and 10 °N (Fig. 7a). Future RCP8.5 changes reveal a dipole pattern with a decrease in rainfall simulated at the beginning of the rainy season and an increase towards the end (Fig. 7c). The Greenland ice sheet melting scenarios amplify these differences (Fig. 7.g-i). For GrIS3m, rainfall decreases during the rainy season at 10 °N (Fig. 7i). For WAIS3m, a slight increase in rainfall is simulated at the beginning of the wet season (Fig. 7e).

For the SAMS, the simulated rainy season lasts from October to April, with large rainfall occurring between 5 °S and 15 °S (Fig 7b). For GrIS1m and GrIS3m changes, a rainfall dipole is shown between the equator and 15 °S (Fig 7h-j). Between January and March rainfall intensifies in the southern part. Conversely, a drying signal is simulated over the northern part in future. In addition, future rainfall significantly increases at the beginning of the rainy season (Oct-Dec). These changes are more pronounced in the GrIS3m experiment (Fig. 7j). For the RCP8.5 and WAIS3m scenarios, future rainfall changes are much weaker (Fig. 7d-f). The RCP8.5 scenario tends to simulate slightly wetter conditions in future (Fig. 7d). The WAIS3m scenario seems to show an opposite pattern with a slight increase in precipitation near the equator and a decrease at 10 °S (Fig. 7f).

https://doi.org/10.5194/egusphere-2022-197
Preprint. Discussion started: 4 May 2022

Over the NAF region, two rainy seasons occur over the Gulf of Guinea (April-May and Oct-Nov), one rainy season occurs over the Sahel (July-Sep) and two rainy seasons occur over East Africa (short rains during Oct-Nov-Dec and long rains in Mar-Apr-May). The ITCZ first reaches the Guinean coast in April-May, moves northward to reach the Sahel during boreal summer and then quickly retreats southward to reach the Guinean coast in Sep-Oct (Fig. 8a). The RCP8.5 and WAIS3m scenarios simulate a slight rainfall increase in April-May nearby the coast (0-5 °N), and a larger increase from Sep to Dec over 0-10 °N (Fig. 8c and Fig. 8e). WAIS3m (Fig. 8e) simulates a larger increase from Sep to Dec with respect to RCP8.5 (Fig. 8c), and the RCP8.5 scenario simulates moderate drier than average conditions at 7 °N during the West African monsoon season (July to Sep). The GrIS1m and GrIS3m scenarios simulate a significant decrease in precipitation over the whole region (Fig. 8g and Fig. 8i). This decrease is larger for the GrIS3m simulation during the West African monsoon season (July-Sep) at 6-10 °N (Fig. 8i), and denotes a southward shift of the ITCZ over NAF.

For the SAF domain, the rainy season extends from October to March and peaks between 10 °S and 15 °S (Fig. 8b). All simulations show an increase in future rainfall between December and May between 15 °S and 5 °S (Fig. 8-d-f-h-j). RCP8.5 (Fig. 8d) and GrIS scenarios (Fig. 8h-j) simulate a rainfall increase at 15 °S-5 °S. The RCP8.5 and WAIS3m scenario simulate drier than average conditions during the onset of the rainy season over southern Africa (Fig. 8d-f). There is a clear southward shift of the ITCZ over the SAF region in GrIS1m and GrIS3m (Fig. 8h-j).

The SAS domain includes both the Indian and South-east Asian monsoons. Depending on the latitude, rainfall is bimodal in the southern part with peaks simulated in March and October-November or uni-modal in the northern part with a peak in August (Fig. 9a). The patterns are very similar between the RCP8.5 (Fig. 9b) and WAIS3m (Fig. 9c) scenarios, with an increase in future precipitation simulated from July to December. The melting of the Greenland ice sheet tends to buffer this increase in rainfall over SAF (Fig. 9d-e).

For the EAS region, although few points show significant differences, there is little difference between the scenarios (Fig. B1). For the AUSMC region, all scenarios simulate an increase in precipitation in the north. This increase extends southwards with the GrIS3m scenario (Fig. B1). See Appendix B for more information.

Our scenarios suggest that a melting of the ice sheet impacts the quantity, the geographical distribution and the seasonality of the precipitation supplied to each monsoon system. However, the studied indicators were calculated at a monthly time step, hence not providing detailed information about frequency and magnitude of potential rainfall extremes and dry spells. In the following we focus on monsoon indicators calculated at a daily time step (see Table 2).

The CDD indicator, representing the length of drought episodes, shows a very large interannual variability for all scenarios and regions (Fig. 10). Nevertheless, a clear increase in the duration of droughts is shown for the GrIS scenarios over the NAMS region (Fig. 10a). Decreases in the duration of the wet season, the number of rainy days per year and total precipitation (CDW, R1mm, Pav) are also shown over NAMS by the GrIS scenarios. Changes in intensity of wet events, characterised by

https://doi.org/10.5194/egusphere-2022-197
Preprint. Discussion started: 4 May 2022

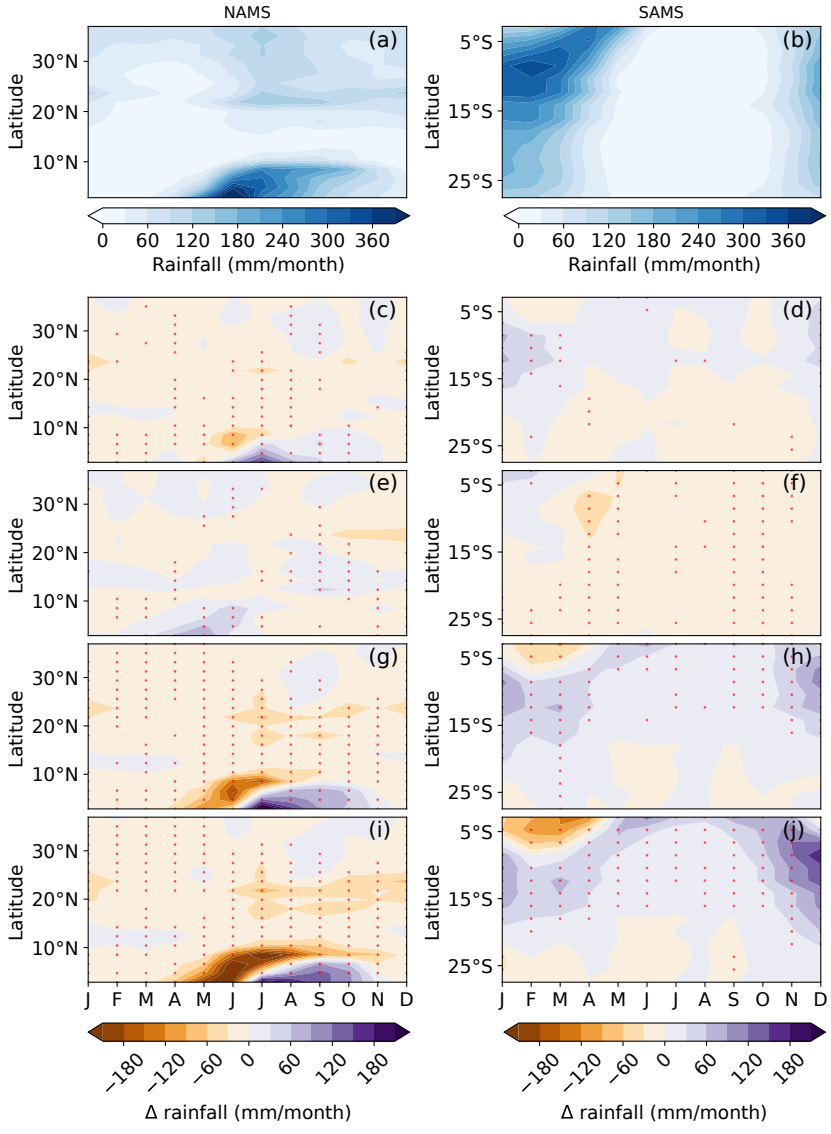

Figure 7. Hovmöller Diagram for the domains of the American continent. The left column corresponds to the NAMS domain (a,c,e,g,i) and the right column to the SAMS domain (b,d,f,h,j). a.b) correspond to the precipitation values in mm month^{-1} over the historical period (1976-2005). All other diagrams correspond to the difference between the future scenario (2041-2070) with c,d) RCP8.5, e,f) WAIS3m, g,h) GrIS1m and i,j) GrIS3m and the historical period (1976-2005), in mm month^{-1}. Significant differences at the 95 % confidence interval are depicted by red dots according to the Wilcoxon-Mann-Whitney test (see Sect. 2.3).

the RX5day and SDII indicators, are moderate over this region (Fig. 10a).

For the SAMS region, changes in CDD are less marked for the GrIS scenarios with respect to the WAIS3m scenario which simulates an increase in cumulative dry days (Fig. 10b). An increase in the intensity of precipitation events is shown over

https://doi.org/10.5194/egusphere-2022-197
Preprint. Discussion started: 4 May 2022

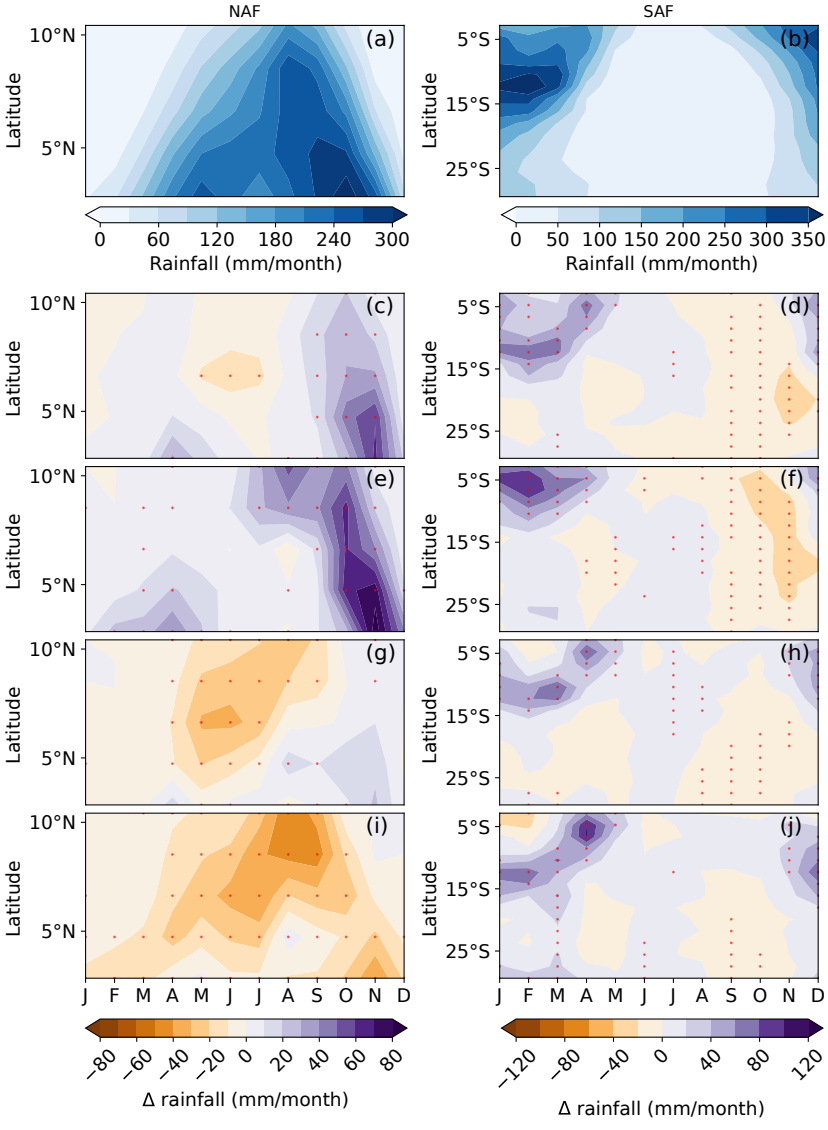

Figure 8. Hovmöller Diagram for the domains of the African continent. The left column corresponds to the NAF domain (a,c,e,g,i) and the right column to the SAF domain (b,d,f,h,j). a.b) correspond to the precipitation values in mm month^{-1} over the historical period (1976-2005). All other diagrams correspond to the difference between the future scenario (2041-2070) with c,d) RCP8.5, e,f) WAIS3m, g,h) GrIS1m and i,j) GrIS3m and the historical period (1976-2005), in mm month^{-1}. Please note that the colour bar values do not correspond to the same values from one column to another. Significant differences at the 95 % confidence interval are depicted by red dots according to the Wilcoxon-Mann-Whitney test (see Sect. 2.3).

340 SAMS (RX5day, SDII), for the RCP8.5 and GrIS scenarios. Interestingly, the WAIS scenario tends to simulate a decrease in

https://doi.org/10.5194/egusphere-2022-197
Preprint. Discussion started: 4 May 2022

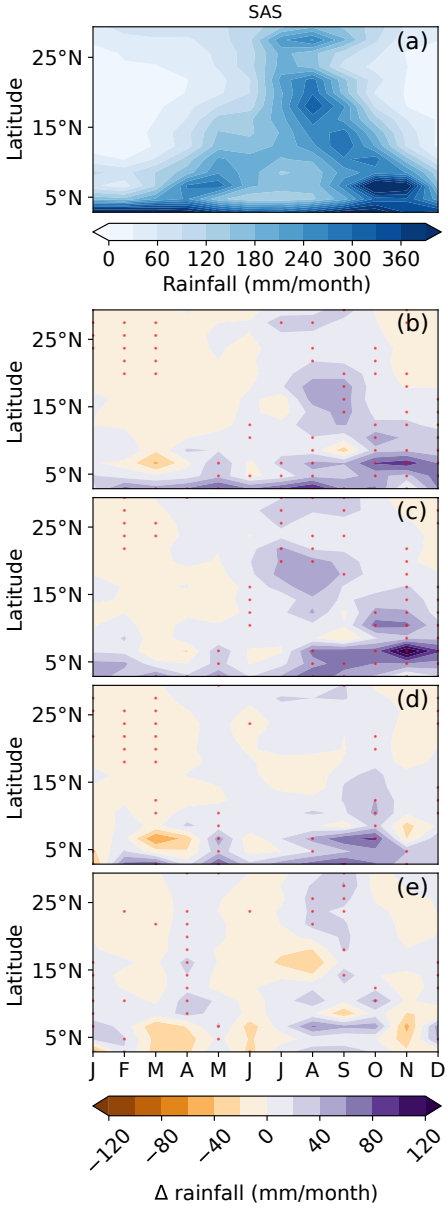

Figure 9. Hovmöller Diagram for the domains of the SAS domain. a) correspond to the precipitation values in mm month^{-1} over the historical period (1976-2005). All other diagrams correspond to the difference between the future scenario (2041-2070) with b) RCP8.5, c) WAIS3m, d) GrIS1m and e) GrIS3m and the historical period (1976-2005), in mm month^{-1}. Significant differences at the 95 % confidence interval are depicted by red dots according to the Wilcoxon-Mann-Whitney test (see Sect. 2.3).

RX5day with respect to the other scenarios. An increase in total annual rainfall (Pav) is also shown over SAMS (Fig. 10b).

https://doi.org/10.5194/egusphere-2022-197
Preprint. Discussion started: 4 May 2022

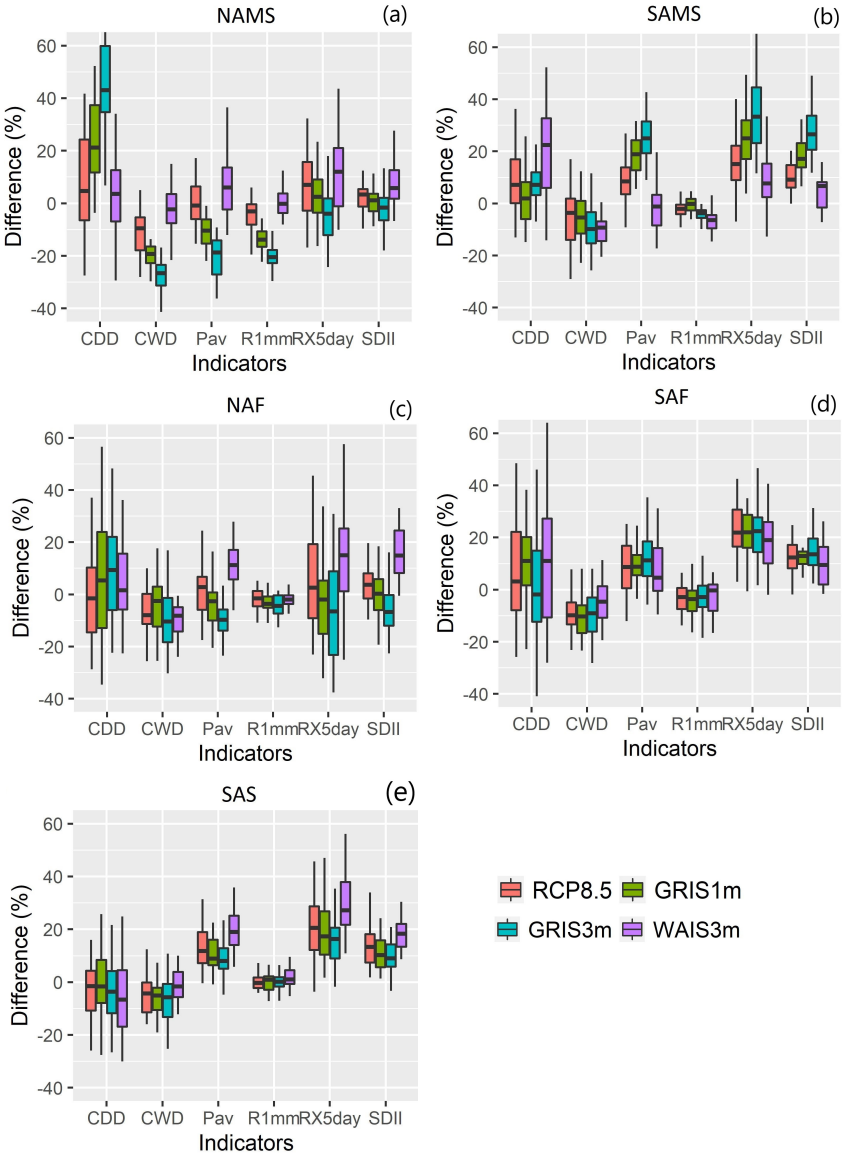

Figure 10. Comparison of the interannual variability of each monsoon index for the period 2041-2070 with the average of the historical period (1976-2005) for each monsoon system a) NAMS, b) SAMS, c) NAF, d) SAF, e) SAS and for each simulation, RCP8.5 in red, GrIS1m in green, GrIS3m in blue and WAIS3m in purple.

Although the interannual variability is very large over the NAF region, the melting of the Greenland ice sheet induce an increase in the number of the CDD and a decrease in the number of the CWD for GrIS3m leading to an overall decrease in

https://doi.org/10.5194/egusphere-2022-197
Preprint. Discussion started: 4 May 2022

annual precipitation (Pav) for the GrIS3m scenario (Fig. 10c). Conversely, an increase in extreme precipitation events (RX5day, SDII) and annual precipitation (Pav) is shown for the WAIS3m scenario. More moderate changes are simulated by the RCP8.5 scenario (Fig. 10c).

In the SAF region, there is an intensification of large precipitation events (RX5day, SDII) and a decrease in the number of cumulative wet days and rainy days (CDW, R1mm) for all simulations (Fig. 10d). Nevertheless, total annual rainfall (Pav) slightly increases for all scenarios (Fig. 10d)

In SAS region, there is an increase in annual precipitation (Pav) for all scenarios linked to an intensification of heavy precipitation events (RX5day, SDII) (Fig. 10e). These changes are largest for the WAIS3M simulation (Fig. 10e).

4 Discussion

We investigated the impact of a partial melting of the ice sheet on monsoons and the associated physical mechanisms using the IPSL-CM5 GCM. This model was forced by three hosing scenarios all considering the RCP8.5 scenario as a common radiative forcing. The WAIS3m experiment simulates a melting of the West Antarctica ice-sheet and the GrIS experiments simulate a partial melting of the Greenland ice sheet equivalent to an additional 1 m and 3 m sea level rise. The Greenland ice sheet, due to its sub-polar position, releases freshwater directly into the North Atlantic, where cold, dense water sinks to form deep currents. This leads to the slowing of the AMOC, as demonstrated in several studies (Stouffer et al., 2006; Swingedouw et al., 2007; Kageyama et al., 2013; Marzin et al., 2013b). The induced collapse of the AMOC, which we consider to be a major disruption of the thermohaline circulation of the oceans (Vellinga and Wood, 2002), does not occur with the RCP8.5 scenario alone. As shown by Weaver et al. (2012), it is unlikely that the AMOC will undergo an abrupt change when only considering standard RCPs scenarios.

The method for water hosing simulations varies greatly from study to study: the amount of water input and salinity can vary, simulations can be carried out at different time-scales for different climatic contexts (paleoclimates, pre-industrial conditions, future GHGs scenarios). The cooling of the North Atlantic induced by the slowing of the AMOC, and the subsequent southward shift of the Atlantic ITCZ are robust results, shown by many climate models (Vellinga and Wood, 2002; Stouffer et al., 2006; Kageyama et al., 2013; Jackson et al., 2015; Liu et al., 2020) and corroborated by climate proxies (Clement and Peterson, 2008; Mulitza et al., 2008; Marzin et al., 2013b).

Previous studies that do not consider a dynamical evolution of GHGs show a cooling of the northern hemisphere, and in some cases a warming of the southern hemisphere (Vellinga and Wood, 2002; Jackson et al., 2015). In our study, the increase in GHGs leads to a standard global warming signal that is buffered by the slowdown of the AMOC. A rapid melting of the West Antarctica ice sheet tends to increase future temperature further at high latitudes in the northern hemisphere during boreal winter. Studies that consider changes in GHGs, suggest that a shut-down of the AMOC might lead to a return to pre-industrial climate conditions (Vellinga and Wood, 2008), which is not the case in the present study. Liu et al. (2020) also use the baseline

https://doi.org/10.5194/egusphere-2022-197
Preprint. Discussion started: 4 May 2022

RCP8.5 scenario to produce climate sensitivity experiments for which they weaken the AMOC. Their findings are consistent with ours, with a lower temperature increase simulated over the northern hemisphere when the AMOC is weakened, a southward shift of the ITCZ and no significant change in the Pacific Ocean. The choice of scenarios and climate models has a strong impact on the robustness of the results. Stouffer et al. (2006) conducted a multi-model analysis in pre-industrial climatic conditions using freshwater inputs of 0.1 Sv and 1 Sv (to compare to 0.22 Sv and 0.68 Sv in our simulations). All climate models simulate a temperature decrease over the Northern Atlantic and Greenland, consistently with our findings, but the responses between climate models vary significantly over the other regions of the Northern Hemisphere. A southward shift of the ITCZ is also simulated by other climate models in their study and this change was robust with the addition of +1 Sv. Pressure gradients change, resulting in a north-south pressure force that pushes the rain belt southward, phenomenon also confirmed by the proxy studies carried out by Mulitza et al. (2008); Marzin et al. (2013b) and Liu et al. (2020).

This latitudinal shift leads to significant changes in African climate, with a drying simulated over the Sahel and increased rainfall simulated over the central and southern part of Africa. These results are consistent with the studies by Mulitza et al. (2008); Kageyama et al. (2013) and Liu et al. (2020). A few paleoclimate studies also show an impact of freshwater inputs on the Indian monsoon (Kageyama et al., 2013; Marzin et al., 2013a), this impact was not evident in our experiments and in results shown by Marzin et al. (2013a). Our study also reveals a southward shift of the American monsoon, with a simulated drying over Central and the Northern part of South America and a large increase in precipitation over the Amazon basin. Jackson et al. (2015) modify the salinity of the North Atlantic Ocean to produce changes equivalent to freshwater inputs of 10 Sv per year for 10 years. This input in freshwater is much larger than the one used in our study, but it shows similar trends for global temperature changes and a southward shift of the ITCZ which also impacts the Indo-Pacific basin. Jackson et al. (2015) also emphasize a drying out of the Amazon, while a strong increase in precipitation is simulated over this region in GrIS experiments, especially during the wet season.

Swingedouw et al. (2008) studied the impact of the Antarctica melting over a longer time period (3000 years). They showed that the melting of Antarctica counteracts climatic changes induced by a melting of northern hemisphere ice-sheet due to a see-saw mechanism, consistently with former findings by Stocker (1998). In our study, freshwater input in the Southern Hemisphere is diluted by the circumpolar current and has varying impacts in different parts of the world. The impacts of northern/southern freshwater inputs have different impacts on the regional monsoon systems.

The IPSL-CM5 model belongs to the CMIP5 intercomparison exercise whose parameterization has evolved for the CMIP6 framework (Boucher et al., 2020). The transition from CMIP5 to CMIP6 has led to changes in many GCMs with reduced biases and uncertainties in many regions of the world. The presence of a double ITCZ is a persistent bias in the different intercomparison exercises, however this bias has reduced in CMIP6 (Tian and Dong, 2020). The representation of monsoons by GCMs has improved between CMIP5 and CMIP6 for China (Xin et al., 2020), India (Gusain et al., 2020), East Asia (Xin et al., 2020), and East Africa, although there are still significant errors (Ayugi et al., 2021). For the Sahel, future rainfall uncertainties

https://doi.org/10.5194/egusphere-2022-197
Preprint. Discussion started: 4 May 2022

remain large despite the evolution of GCMs (Monerie et al., 2020). For Central America, and South America, there is a large dispersion across the different climate models utilized in CMIP5 and CMIP6, with however a slight improvement in CMIP6 GCMs (Ortega et al., 2021). It is noteworthy that the multi-model average is often closer to reality than each model considered independently (Ayugi et al., 2021). Significant changes in rainfall seasonality are simulated by the IPSL-CM5 model as well as in the CMIP5 and CMIP6 intercomparison exercises (Wainwright et al., 2021). In our methodological framework, freshwater input is added continuously between 2020 and 2070. However, the melting and release of freshwater might be highly non-linear (tipping point) and may vary seasonally. Sensitivity climate experiments that consider different values of freshwater input depending on the season would allow a more realistic simulation. Although the transition from CMIP5 to CMIP6 has led to improvements in climate simulation in many regions of the world, the models still have systematic errors in the simulation of precipitation. The IPSL-CM5 model, like other GCMs, shows a significant bias with the presence of a double ITCZ.

The most extreme emission scenario, RCP8.5, was used in this study. The choice of RCP8.5 as a credible scenario for the 21^{st} century has been recently criticized by Hausfather and Peters (2020). Hausfather and Peters (2020) argue that the real word GHGs emissions, in order to reach the RCP8.5 scenario, would require an increase in coal use beyond recoverable and available reserves. They also note that even without climate policies, as assumed in RCP8.5, clean energy costs tend to decrease over time. Consequently, they advise that the RCP8.5 scenario should not be used as a most likely future scenario, but only as an extreme one (Hausfather and Peters, 2020). The potential large number of retroactive events in snow-covered regions resulting from rising temperatures (Fettweis et al., 2012) suggest that tipping points can be very rapid and sudden. Recent trends are worrying: the recent melting of the A68 iceberg was estimated to have released about 152 Gt of fresh water and nutrients near South Georgia (Braakmann-Folgmann et al., 2022). In addition, nearly twice as much lightning was detected north of 80° N in 2021, than in the previous nine years combined, denoting an increase in liquid precipitation at high latitudes (Network, 2022). We only investigated the impact of ice-sheet melting, but a melting of the permafrost, which would potentially release a large amount of methane in the atmosphere, is worth investigating (Stendel and Christensen, 2002). As perspectives, multi-model studies of tipping point scenarios (ice sheet melting, melting of the permafrost, dieback of the Amazon...) and their potential impacts on societies, should be encouraged (Lenton et al., 2019). Rising sea levels and induced climatic impacts could have primordial consequences for human societies, health (Chemison et al., 2021), agriculture (Defrance et al., 2017) and the global economy (Kuhlbrodt et al., 2009).

https://doi.org/10.5194/egusphere-2022-197
Preprint. Discussion started: 4 May 2022

Appendix A: Ocean dynamics

The difference in stream function between future and historical periods is slight affected by seasonality in our simulations (Fig. A1 and Fig. A2). Our simulation provides continuous freshwater between 2020 and 2070 without seasonal variations. This may explain why there is small seasonal difference for the simulations with ice melt (Fig. A1b-c-d and Fig. A2b-c-d). The GrIS1m and GrIS3m simulations still show larger maximum differences during the boreal summer located in the northern hemisphere (Fig. A1c-d and Fig.A2c-d). In contrast, for the southern hemisphere, the maximum difference for the GrIS simulations appears to be reached during boreal winter (Fig. A1c-d and Fig. A2c-d).

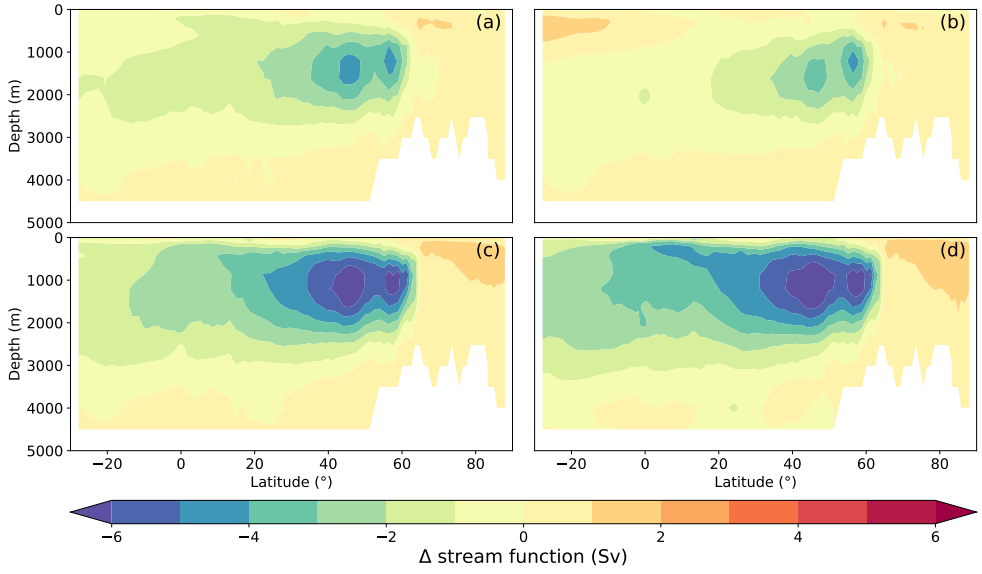

Figure A1. Stream function difference between future scenarios (2041-2070) and historical simulation (1976-2005) for MJJAS season. The future scenarios are a) RCP8.5, b) WAIS3m, c) GrIS1m and d) GrIS3m.

https://doi.org/10.5194/egusphere-2022-197
Preprint. Discussion started: 4 May 2022

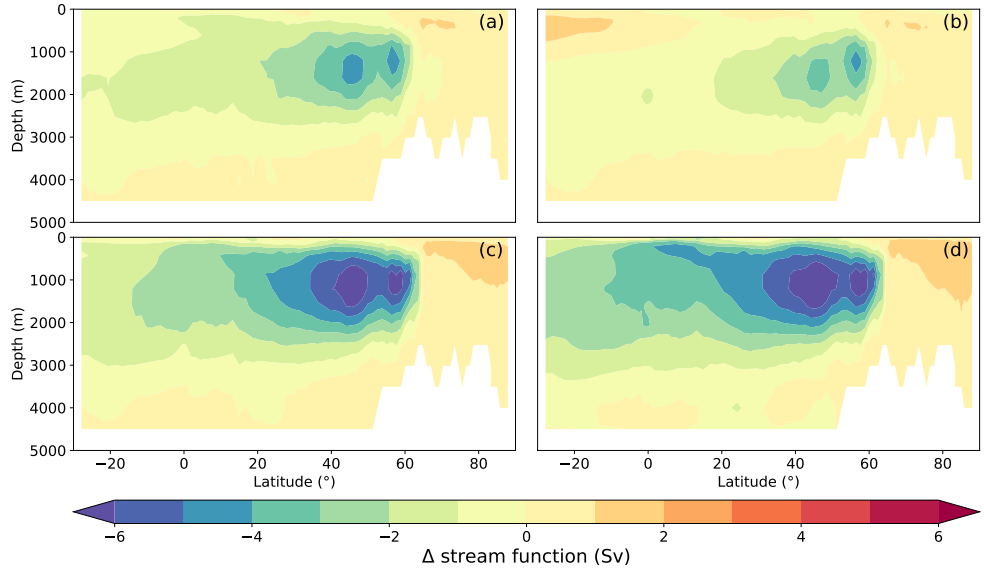

Figure A2. Stream function difference between future scenarios (2041-2070) and historical simulation (1976-2005) for NDJFM season. The future scenarios are a) RCP8.5, b) WAIS3m, c) GrIS1m and d) GrIS3m.

Appendix B: Impact on regional monsoons

For the EAS region, the wet season extends from May to August with maximum rainfall simulated over the south in July (Fig. B1a). Although only a few points show significant differences, there is still little difference between the scenarios when comparing future and historical periods. All experiments simulate a decrease in precipitation during boreal winter. During summer, there is an increase in precipitation in the north. In the south, there is a decrease in precipitation during winter but also at the beginning of the wet season, whereas there is an increase in precipitation at the end of the wet season. (Fig. B1c-e-g-i).

https://doi.org/10.5194/egusphere-2022-197
Preprint. Discussion started: 4 May 2022

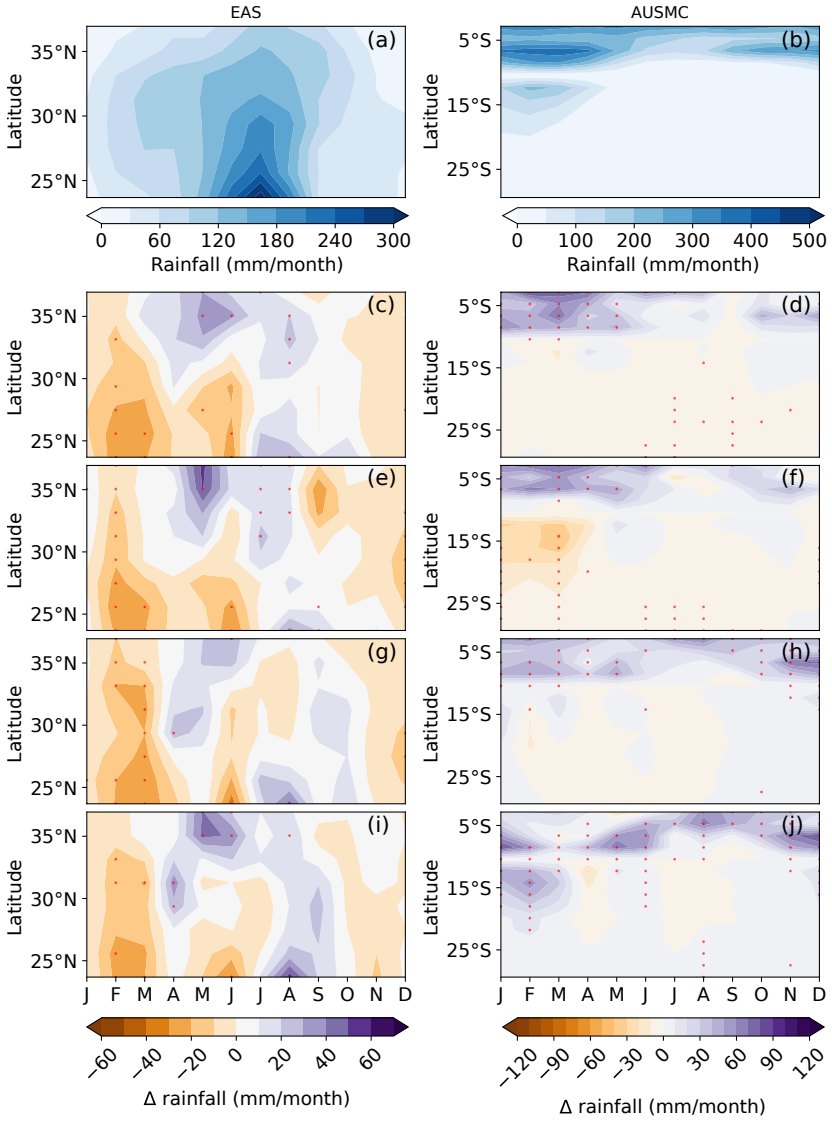

Figure B1. Hovmöller Diagram. The left column corresponds to the EAS domain (a,c,e,g,i) and the right column to the AUSMC domain (b,d,f,h,j). a.b) correspond to the precipitation values in mm month^{-1} over the historical period (1976-2005). All other diagrams correspond to the difference between the future scenario (2041-2070) with c,d) RCP8.5, e,f) WAIS3m, g,h) GrIS1m and i,j) GrIS3m and the historical period (1976-2005). Significant differences at the 95 % confidence interval are depicted by red dots according to the Wilcoxon-Mann-Whitney test (see 2.3).

To validate the use of the different monsoon indicators for each study region, indices for the historical period are compared with those obtained for the EWEMBII data. For CDD, the values obtained are close between the two datasets, although the values from the historical simulations have a slight negative bias for the East Asian, North American and South African regions (Fig. B2a). For the CDW, all regions have a slight negative bias with the historical simulation (Fig. B2b). This bias is

https://doi.org/10.5194/egusphere-2022-197
Preprint. Discussion started: 4 May 2022

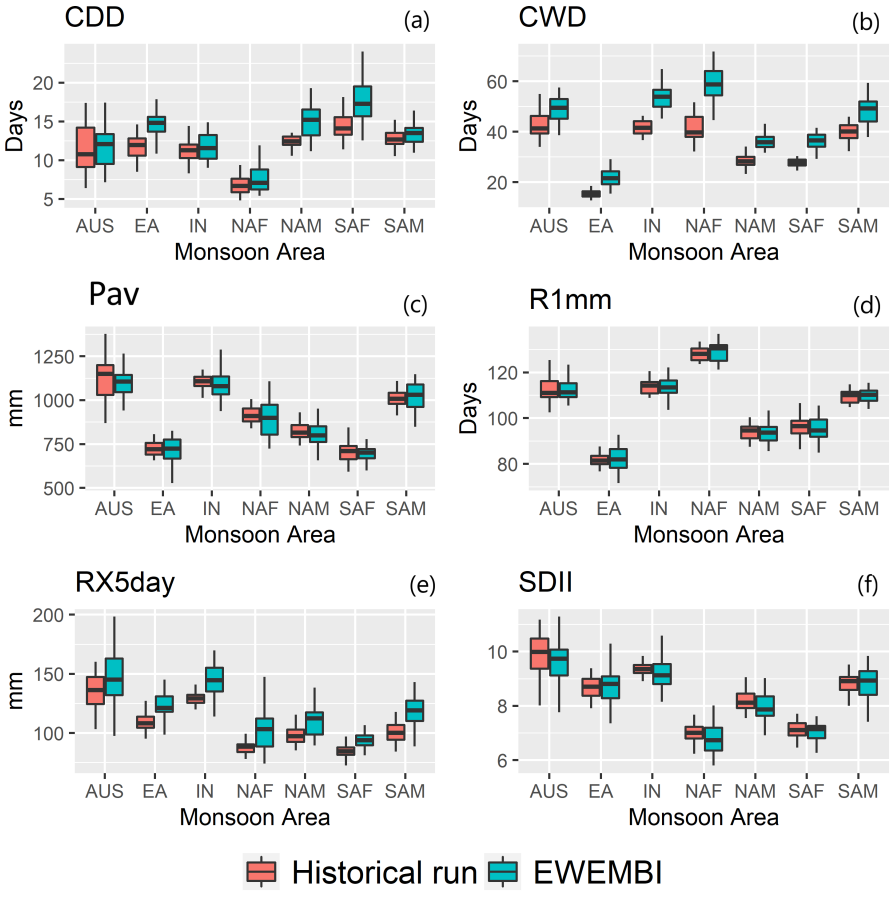

Figure B2. Comparison of the interannual variability of each monsoon index for the period 1976-2005 for historical run simulation (red) and EWEMBI data (blue) for each monsoon system and for each monsoon indicator, a) CDD, b) CDW, c) Pav, d) R1mm, e) RX5day, f) SDII.

also shown for the RX5day indicator (Fig. B2e) but is not found with the Pav, R1mm, SDII indicators which have very similar values between the two data sets (Fig. B2c-d-f). Despite a slight negative bias for some indicators in some regions, the indicators show the same trends between the two datasets (Fig. B2).

For the EAS region, there are almost no changes in the different monsoon indexes for all scenarios, only a slight increase in total precipitation (Pav) due to an intensification of precipitation events (RX5day, SDII) (Fig. B3a).

For AUSMC region, a very high inter-annual variability is shown (Fig. B3b). Total precipitation (Pav) increases slightly for the RCP8.5, GrIS1m and GrIS3m scenarios, which may be related to a decrease in the duration of the dry season (CDD) and an intensification of precipitation events (RX5day, SDII) (Fig. B3b).

https://doi.org/10.5194/egusphere-2022-197
Preprint. Discussion started: 4 May 2022

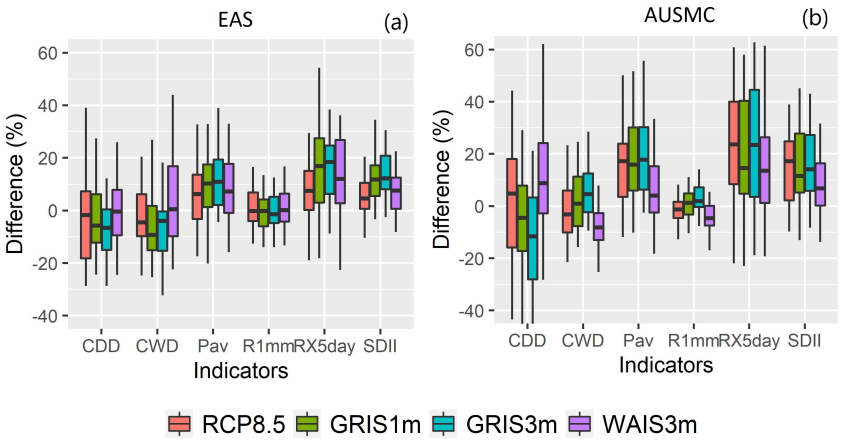

Figure B3. Comparison of the interannual variability of each monsoon index for the period 2041-2070 with the average of the historical period (1976-2005) for each monsoon system a) EAS, b) AUSMC.

Data availability. All simulations that support the findings of this study are available at https://doi.org/10.17605/OSF.IO/YTER9 that should allow reproducibility of the main figures.

Author contributions. A.C. wrote the article, produced most of the figures and analysis. D.D. carried out the WAIS3m, GrIS1m and GrIS3m simulations and produced figures. G.R. and C.C. guided to the analysis and contributed to the writing of the paper.

Competing interests. The authors declare no competing interests.

Acknowledgements. We acknowledge the Direction de la Recherche Fondamentale (DRF) of the Commissariat à l'énergie atomique et aux énergies alternatives (CEA) for A.C. PhD funding and the DRF Impulsion program for funding the EPICLIM project awarded to G.R.

https://doi.org/10.5194/egusphere-2022-197
Preprint. Discussion started: 4 May 2022

References

Adler, R. F., Sapiano, M. R., Huffman, G. J., Wang, J.-J., Gu, G., Bolvin, D., Chiu, L., Schneider, U., Becker, A., Nelkin, E., et al.: The Global Precipitation Climatology Project (GPCP) monthly analysis (new version 2.3) and a review of 2017 global precipitation, Atmosphere, 9, 138, https://doi.org/10.3390/atmos9040138, 2018.

Aumont, O. and Bopp, L.: Globalizing results from ocean in situ iron fertilization studies, Global Biogeochemical Cycles, 20, https://doi.org/10.1029/2005GB002591, 2006.

Ayugi, B., Jiang, Z., Zhu, H., Ngoma, H., Babaousmail, H., Karim, R., and Dike, V.: Comparison of CMIP6 and CMIP5 models in simulating mean and extreme precipitation over East Africa, International Journal of Climatology, https://doi.org/10.1002/joc.7207, 2021.

Bakker, P., Schmittner, A., Lenaerts, J., Abe-Ouchi, A., Bi, D., van den Broeke, M., Chan, W.-L., Hu, A., Beadling, R., Marsland, S., et al.: Fate of the Atlantic Meridional Overturning Circulation: Strong decline under continued warming and Greenland melting, Geophysical Research Letters, 43, 12–252, https://doi.org/10.1002/2016GL070457, 2016.

Biasutti, M. and Sobel, A. H.: Delayed Sahel rainfall and global seasonal cycle in a warmer climate, Geophysical Research Letters, 36, https://doi.org/10.1029/2009GL041303, 2009.

Boucher, O., Servonnat, J., Albright, A. L., Aumont, O., Balkanski, Y., Bastrikov, V., Bekki, S., Bonnet, R., Bony, S., Bopp, L., et al.: Presentation and evaluation of the IPSL-CM6A-LR climate model, Journal of Advances in Modeling Earth Systems, 12, e2019MS002 010, https://doi.org/10.1029/2019MS002010, 2020.

Braakmann-Folgmann, A., Shepherd, A., Gerrish, L., Izzard, J., and Ridout, A.: Observing the disintegration of the A68A iceberg from space, Remote Sensing of Environment, 270, 112 855, https://doi.org/10.1016/j.rse.2021.112855, 2022.

Broecker, W., Bond, G., Klas, M., Clark, E., and McManus, J.: Origin of the northern Atlantic's Heinrich events, Climate Dynamics, 6, 265–273, https://doi.org/10.1007/BF00193540, 1992.

Cavazos, T., Turrent, C., and Lettenmaier, D.: Extreme precipitation trends associated with tropical cyclones in the core of the North American monsoon, Geophysical Research Letters, 35, https://doi.org/10.1029/2008GL035832, 2008.

Chemison, A., Ramstein, G., Tompkins, A. M., Defrance, D., Camus, G., Charra, M., and Caminade, C.: Impact of an accelerated melting of Greenland on malaria distribution over Africa, Nature Communications, 12, 1–12, https://doi.org/10.1038/s41467-021-24134-4, 2021.

Chemison, A., Defrance, D., Ramstein, G., and Caminade, C.: Simulation files to reproduce the paper "Impact of an acceleration of ice sheet melting on monsoon systems", https://doi.org/10.17605/OSF.IO/YTER9, 2022.

Cheng, W., Chiang, J. C., and Zhang, D.: Atlantic meridional overturning circulation (AMOC) in CMIP5 models: RCP and historical simulations, Journal of Climate, 26, 7187–7197, https://doi.org/10.1175/JCLI-D-12-00496.1, 2013.

Christensen, J. H., Kanikicharla, K. K., Aldrian, E., An, S. I., Cavalcanti, I. F. A., de Castro, M., Dong, W., Goswami, P., Hall, A., Kanyanga, J. K., et al.: Climate phenomena and their relevance for future regional climate change, in: Climate change 2013 the physical science basis: Working group I contribution to the fifth assessment report of the intergovernmental panel on climate change, pp. 1217–1308, Cambridge University Press, https://doi.org/10.1017/CBO9781107415324.028, 2013.

Church, J. A., Clark, P. U., Cazenave, A., Gregory, J. M., Jevrejeva, S., Levermann, A., Merrifield, M. A., Milne, G. A., Nerem, R. S., Nunn, P. D., et al.: Sea level change, Tech. rep., PM Cambridge University Press, 2013.

Clement, A. C. and Peterson, L. C.: Mechanisms of abrupt climate change of the last glacial period, Reviews of Geophysics, 46, https://doi.org/10.1029/2006RG000204, 2008.

https://doi.org/10.5194/egusphere-2022-197
Preprint. Discussion started: 4 May 2022

Cook, B. I. and Seager, R.: The response of the North American Monsoon to increased greenhouse gas forcing, Journal of Geophysical Research: Atmospheres, 118, 1690–1699, https://doi.org/10.1002/jgrd.50111, 2013.

DeConto, R. M. and Pollard, D.: Contribution of Antarctica to past and future sea-level rise, Nature, 531, 591–597, https://doi.org/10.1038/nature17145, 2016.

Defrance, D., Ramstein, G., Charbit, S., Vrac, M., Famien, A. M., Sultan, B., Swingedouw, D., Dumas, C., Gemenne, F., Alvarez-Solas, J., et al.: Consequences of rapid ice sheet melting on the Sahelian population vulnerability, Proceedings of the National Academy of Sciences, 114, 6533–6538, https://doi.org/10.1073/pnas.1619358114, 2017.

Defrance, D., Catry, T., Rajaud, A., Dessay, N., and Sultan, B.: Impacts of Greenland and Antarctic Ice Sheet melt on future Köppen climate zone changes simulated by an atmospheric and oceanic general circulation model, Applied Geography, 119, 102 216, https://doi.org/10.1016/j.apgeog.2020.102216, 2020.

Duffy, P. and Tebaldi, C.: Increasing prevalence of extreme summer temperatures in the US, Climatic Change, 111, 487–495, https://doi.org/10.1007/s10584-012-0396-6, 2012.

Dufresne, J.-L., Foujols, M.-A., Denvil, S., Caubel, A., Marti, O., Aumont, O., Balkanski, Y., Bekki, S., Bellenger, H., Benshila, R., et al.: Climate change projections using the IPSL-CM5 Earth System Model: from CMIP3 to CMIP5, Climate Dynamics, 40, 2123–2165, https://doi.org/10.1007/s00382-012-1636-1, 2013.

Dunning, C. M., Black, E., and Allan, R. P.: Later wet seasons with more intense rainfall over Africa under future climate change, Journal of Climate, 31, 9719–9738, https://doi.org/10.1175/JCLI-D-18-0102.1, 2018.

Fettweis, X., Franco, B., Tedesco, M., Van Angelen, J., Lenaerts, J. T., van den Broeke, M. R., and Gallée, H.: Estimating Greenland ice sheet surface mass balance contribution to future sea level rise using the regional atmospheric climate model MAR, Cryosphere discussions, 6, 3101–3147, https://doi.org/10.5194/tc-7-469-2013, 2012.

Fichefet, T. and Maqueda, M. M.: Sensitivity of a global sea ice model to the treatment of ice thermodynamics and dynamics, Journal of Geophysical Research: Oceans, 102, 12 609–12 646, https://doi.org/10.1029/97JC00480, 1997.

Gillet-Chaulet, F., Gagliardini, O., Seddik, H., Nodet, M., Durand, G., Ritz, C., Zwinger, T., Greve, R., and Vaughan, D. G.: Greenland ice sheet contribution to sea-level rise from a new-generation ice-sheet model, The Cryosphere, 6, 1561–1576, https://doi.org/10.5194/tc-6-1561-2012, 2012.

Gusain, A., Ghosh, S., and Karmakar, S.: Added value of CMIP6 over CMIP5 models in simulating Indian summer monsoon rainfall, Atmospheric Research, 232, 104 680, https://doi.org/10.1016/j.atmosres.2019.104680, 2020.

Hansen, J., Sato, M., Hearty, P., Ruedy, R., Kelley, M., Masson-Delmotte, V., Russell, G., Tselioudis, G., Cao, J., Rignot, E., et al.: Ice melt, sea level rise and superstorms: evidence from paleoclimate data, climate modeling, and modern observations that 2 C global warming could be dangerous, Atmospheric Chemistry and Physics, 16, 3761–3812, https://doi.org/10.5194/acp-16-3761-2016, 2016.

Hauglustaine, D., Hourdin, F., Jourdain, L., Filiberti, M.-A., Walters, S., Lamarque, J.-F., and Holland, E.: Interactive chemistry in the Laboratoire de Météorologie Dynamique general circulation model: Description and background tropospheric chemistry evaluation, Journal of Geophysical Research: Atmospheres, 109, https://doi.org/10.1029/2003JD003957, 2004.

Hausfather, Z. and Peters, G. P.: Emissions–the 'business as usual'story is misleading, https://doi.org/10.1038/d41586-020-00177-3, 2020.

Hemming, S. R.: Heinrich events: Massive late Pleistocene detritus layers of the North Atlantic and their global climate imprint, Reviews of Geophysics, 42, https://doi.org/10.1029/2003RG000128, 2004.

https://doi.org/10.5194/egusphere-2022-197
Preprint. Discussion started: 4 May 2022

Hourdin, F., Foujols, M.-A., Codron, F., Guemas, V., Dufresne, J.-L., Bony, S., Denvil, S., Guez, L., Lott, F., Ghattas, J., et al.: Impact of the LMDZ atmospheric grid configuration on the climate and sensitivity of the IPSL-CM5A coupled model, Climate Dynamics, 40, 2167–2192, https://doi.org/10.1007/s00382-012-1411-3, 2013.

Hsu, P.-c., Li, T., Murakami, H., and Kitoh, A.: Future change of the global monsoon revealed from 19 CMIP5 models, Journal of Geophysical Research: Atmospheres, 118, 1247–1260, https://doi.org/10.1002/jgrd.50145, 2013.

Hurtt, G. C., Chini, L. P., Frolking, S., Betts, R., Feddema, J., Fischer, G., Fisk, J., Hibbard, K., Houghton, R., Janetos, A., et al.: Harmonization of land-use scenarios for the period 1500–2100: 600 years of global gridded annual land-use transitions, wood harvest, and resulting secondary lands, Climatic change, 109, 117, https://doi.org/10.1007/s10584-011-0153-2, 2011.

Jackson, L., Kahana, R., Graham, T., Ringer, M., Woollings, T., Mecking, J., and Wood, R.: Global and European climate impacts of a slowdown of the AMOC in a high resolution GCM, Climate dynamics, 45, 3299–3316, https://doi.org/10.1007/s00382-015-2540-2, 2015.

Jiang, Z., Song, J., Li, L., Chen, W., Wang, Z., and Wang, J.: Extreme climate events in China: IPCC-AR4 model evaluation and projection, Climatic Change, 110, 385–401, https://doi.org/10.1007/s10584-011-0090-0, 2012.

Jones, C. and Carvalho, L. M.: Climate change in the South American monsoon system: present climate and CMIP5 projections, Journal of Climate, 26, 6660–6678, https://doi.org/10.1175/JCLI-D-12-00412.1, 2013.

Jourdain, N. C., Gupta, A. S., Taschetto, A. S., Ummenhofer, C. C., Moise, A. F., and Ashok, K.: The Indo-Australian monsoon and its relationship to ENSO and IOD in reanalysis data and the CMIP3/CMIP5 simulations, Climate dynamics, 41, 3073–3102, https://doi.org/10.1007/s00382-013-1676-1, 2013.

Kageyama, M., Merkel, U., Otto-Bliesner, B., Prange, M., Abe-Ouchi, A., Lohmann, G., Ohgaito, R., Roche, D., Singarayer, J., Swingedouw, D., et al.: Climatic impacts of fresh water hosing under Last Glacial Maximum conditions: a multi-model study, Climate of the Past, 9, 935–953, https://doi.org/10.5194/cp-9-935-2013, 2013.

Kitoh, A., Endo, H., Krishna Kumar, K., Cavalcanti, I. F., Goswami, P., and Zhou, T.: Monsoons in a changing world: A regional perspective in a global context, Journal of Geophysical Research: Atmospheres, 118, 3053–3065, https://doi.org/10.1002/jgrd.50258, 2013.

Krinner, G., Viovy, N., de Noblet-Ducoudré, N., Ogée, J., Polcher, J., Friedlingstein, P., Ciais, P., Sitch, S., and Prentice, I. C.: A dynamic global vegetation model for studies of the coupled atmosphere-biosphere system, Global Biogeochemical Cycles, 19, https://doi.org/10.1029/2003GB002199, 2005.

Krinner, G., Lézine, A.-M., Braconnot, P., Sepulchre, P., Ramstein, G., Grenier, C., and Gouttevin, I.: A reassessment of lake and wetland feedbacks on the North African Holocene climate, Geophysical Research Letters, 39, https://doi.org/10.1029/2012GL050992, 2012.

Kuhlbrodt, T., Rahmstorf, S., Zickfeld, K., Vikebø, F. B., Sundby, S., Hofmann, M., Link, P. M., Bondeau, A., Cramer, W., and Jaeger, C.: An integrated assessment of changes in the thermohaline circulation, Climatic Change, 96, 489–537, https://doi.org/10.1007/s10584-009-9561-y, 2009.

Lange, S.: EartH2Observe, WFDEI and ERA-Interim data Merged and Bias-corrected for ISIMIP (EWEMBI), https://doi.org/10.5880/pik.2016.004, 2016.

Lau, K.-M., Ramanathan, V., Wu, G.-X., Li, Z., Tsay, S., Hsu, C., Sikka, R., Holben, B., Lu, D., Tartari, G., et al.: The Joint Aerosol–Monsoon Experiment: A new challenge for monsoon climate research, Bulletin of the American Meteorological Society, 89, 369–384, https://doi.org/10.1175/BAMS-89-3-369, 2008.

Lean, J., Rottman, G., Harder, J., and Kopp, G.: SORCE contributions to new understanding of global change and solar variability, in: The Solar Radiation and Climate Experiment (SORCE), pp. 27–53, Springer, https://doi.org/10.1007/0-387-37625-9_3, 2005.

https://doi.org/10.5194/egusphere-2022-197
Preprint. Discussion started: 4 May 2022

Lee, J.-Y. and Wang, B.: Future change of global monsoon in the CMIP5, Climate Dynamics, 42, 101–119, https://doi.org/10.1007/s00382-012-1564-0, 2014.

Lee, J.-Y., Marotzke, J., Bala, G., Cao, L., Corti, S., Dunne, J. P., Engelbrecht, F., Fischer, E. M., Fyfe, J., Jones, C., et al.: Future global climate: scenario-based projections and near-term information, in: AGU Fall Meeting 2021, AGU, 2021.

Lefevre, F., Brasseur, G., Folkins, I., Smith, A., and Simon, P.: Chemistry of the 1991–1992 stratospheric winter: Three-dimensional model simulations, Journal of Geophysical Research: Atmospheres, 99, 8183–8195, https://doi.org/10.1029/93JD03476, 1994.

Lenton, T. M., Rockström, J., Gaffney, O., Rahmstorf, S., Richardson, K., Steffen, W., and Schellnhuber, H. J.: Climate tipping points—too risky to bet against, https://doi.org/10.1038/d41586-019-03595-0, 2019.

Li, X., Ting, M., Li, C., and Henderson, N.: Mechanisms of Asian summer monsoon changes in response to anthropogenic forcing in CMIP5 models, Journal of Climate, 28, 4107–4125, https://doi.org/10.1175/JCLI-D-14-00559.1, 2015.

Liu, W., Fedorov, A. V., Xie, S.-P., and Hu, S.: Climate impacts of a weakened Atlantic Meridional Overturning Circulation in a warming climate, Science advances, 6, eaaz4876, https://doi.org/10.1126/sciadv.aaz4876, 2020.

Madec, G., Bourdallé-Badie, R., Bouttier, P.-A., Bricaud, C., Bruciaferri, D., Calvert, D., Chanut, J., Clementi, E., Coward, A., Delrosso, D., et al.: NEMO ocean engine, NEMO ocean engine, https://doi.org/10.5281/zenodo.3248739, 2017.

Mariotti, L., Diallo, I., Coppola, E., and Giorgi, F.: Seasonal and intraseasonal changes of African monsoon climates in 21st century CORDEX projections, Climatic change, 125, 53–65, https://doi.org/10.1007/s10584-014-1097-0, 2014.

Marzin, C., Braconnot, P., and Kageyama, M.: Relative impacts of insolation changes, meltwater fluxes and ice sheets on African and Asian monsoons during the Holocene, Climate dynamics, 41, 2267–2286, https://doi.org/10.1007/s00382-013-1948-9, 2013a.

Marzin, C., Kallel, N., Kageyama, M., Duplessy, J.-C., and Braconnot, P.: Glacial fluctuations of the Indian monsoon and their relationship with North Atlantic climate: new data and modelling experiments, Climate of the Past, 9, 2135–2151, https://doi.org/10.5194/cp-9-2135-2013, 2013b.

Meehl, G. A., Boer, G. J., Covey, C., Latif, M., and Stouffer, R. J.: The coupled model intercomparison project (CMIP), Bulletin of the American Meteorological Society, 81, 313–318, http://www.jstor.org/stable/26215108, 2000.

Mimura, N.: Sea-level rise caused by climate change and its implications for society, Proceedings of the Japan Academy, Series B, 89, 281–301, https://doi.org/10.2183/pjab.89.281, 2013.

Monerie, P.-A., Wainwright, C. M., Sidibe, M., and Akinsanola, A. A.: Model uncertainties in climate change impacts on Sahel precipitation in ensembles of CMIP5 and CMIP6 simulations, Climate Dynamics, 55, 1385–1401, https://doi.org/10.1007/s00382-020-05332-0, 2020.

Moss, R. H., Edmonds, J. A., Hibbard, K. A., Manning, M. R., Rose, S. K., Van Vuuren, D. P., Carter, T. R., Emori, S., Kainuma, M., Kram, T., et al.: The next generation of scenarios for climate change research and assessment, Nature, 463, 747–756, https://doi.org/10.1038/nature08823, 2010.

Mulitza, S., Prange, M., Stuut, J.-B., Zabel, M., Von Dobeneck, T., Itambi, A. C., Nizou, J., Schulz, M., and Wefer, G.: Sahel megadroughts triggered by glacial slowdowns of Atlantic meridional overturning, Paleoceanography, 23, https://doi.org/10.1029/2008PA001637, 2008.

Network, V. L. D.: Total Lightning Statistics 2021: Vaisala Annual Lightning Report, 2022.

Ortega, G., Arias, P. A., Villegas, J. C., Marquet, P. A., and Nobre, P.: Present-day and future climate over central and South America according to CMIP5/CMIP6 models, International Journal of Climatology, https://doi.org/10.1002/joc.7221, 2021.

Peterson, B. J., McClelland, J., Curry, R., Holmes, R. M., Walsh, J. E., and Aagaard, K.: Trajectory shifts in the Arctic and subarctic freshwater cycle, Science, 313, 1061–1066, https://doi.org/10.1126/science.1122593, 2006.

https://doi.org/10.5194/egusphere-2022-197
Preprint. Discussion started: 4 May 2022

Ranasinghe, R., A C, R., R, V., N, A., E, C., F.A, C., S, D., A.S, I., M, R., D, R. C., J, S., M.B, S., C, T., W, W., and R, Z.: Climate Change Information for Regional Impact and for Risk Assessment, in: In Climate Change 2021: The Physical Science Basis. Contribution of Working Group I to the Sixth Assessment Report of the Intergovernmental Panel on Climate Change, 2021.

Rignot, E., Velicogna, I., van den Broeke, M. R., Monaghan, A., and Lenaerts, J. T.: Acceleration of the contribution of the Greenland and Antarctic ice sheets to sea level rise, Geophysical Research Letters, 38, https://doi.org/10.1029/2011GL046583, 2011.

Schiller, A., Mikolajewicz, U., and Voss, R.: The stability of the North Atlantic thermohaline circulation in a coupled ocean-atmosphere general circulation model, Climate Dynamics, 13, 325–347, https://doi.org/10.1007/s003820050169, 1997.

Seneviratne, S. I., Wilhelm, M., Stanelle, T., van den Hurk, B., Hagemann, S., Berg, A., Cheruy, F., Higgins, M. E., Meier, A., Brovkin, V., et al.: Impact of soil moisture-climate feedbacks on CMIP5 projections: First results from the GLACE-CMIP5 experiment, Geophysical Research Letters, 40, 5212–5217, https://doi.org/10.1002/grl.50956, 2013.

Shongwe, M. E., van Oldenborgh, G. J., Van den Hurk, B., and van Aalst, M.: Projected changes in mean and extreme precipitation in Africa under global warming. Part II: East Africa, Journal of climate, 24, 3718–3733, https://doi.org/10.1175/2010JCLI2883.1, 2011.

Sillmann, J., Kharin, V., Zhang, X., Zwiers, F., and Bronaugh, D.: Climate extremes indices in the CMIP5 multimodel ensemble: Part 1. Model evaluation in the present climate, Journal of Geophysical Research: Atmospheres, 118, 1716–1733, https://doi.org/10.1002/jgrd.50203, 2013.

Stendel, M. and Christensen, J.: Impact of global warming on permafrost conditions in a coupled GCM, Geophysical Research Letters, 29, 10–1, https://doi.org/10.1029/2001GL014345, 2002.

Stocker, T. F.: The seesaw effect, Science, 282, 61–62, https://doi.org/10.1126/science.282.5386.61, 1998.

Stouffer, R. J., Yin, J., Gregory, J., Dixon, K., Spelman, M., Hurlin, W., Weaver, A., Eby, M., Flato, G., Hasumi, H., et al.: Investigating the causes of the response of the thermohaline circulation to past and future climate changes, Journal of climate, 19, 1365–1387, https://doi.org/10.1175/JCLI3689.1, 2006.

Suhaila, J., Deni, S. M., Wan Zin, W. Z., and Jemain, A. A.: Spatial patterns and trends of daily rainfall regime in Peninsular Malaysia during the southwest and northeast monsoons: 1975–2004, Meteorology and Atmospheric Physics, 110, 1–18, https://doi.org/10.1007/s00703-010-0108-6, 2010.

Swingedouw, D., Braconnot, P., and Schmittner, A.: Effect of the Greenland ice-sheet melting on the response and stability of the AMOC in the next centuries, GEOPHYSICAL MONOGRAPH-AMERICAN GEOPHYSICAL UNION, 173, 383, https://doi.org/10.1029/173GM24, 2007.

Swingedouw, D., Fichefet, T., Huybrechts, P., Goosse, H., Driesschaert, E., and Loutre, M.-F.: Antarctic ice-sheet melting provides negative feedbacks on future climate warming, Geophysical Research Letters, 35, https://doi.org/10.1029/2008GL034410, 2008.

Swingedouw, D., Fichefet, T., Goosse, H., and Loutre, M.-F.: Impact of transient freshwater releases in the Southern Ocean on the AMOC and climate, Climate dynamics, 33, 365–381, https://doi.org/10.1007/s00382-008-0496-1, 2009a.

Swingedouw, D., Mignot, J., Braconnot, P., Mosquet, E., Kageyama, M., and Alkama, R.: Impact of freshwater release in the North Atlantic under different climate conditions in an OAGCM, Journal of Climate, 22, 6377–6403, https://doi.org/10.1175/2009JCLI3028.1, 2009b.

Swingedouw, D., Rodehacke, C. B., Behrens, E., Menary, M., Olsen, S. M., Gao, Y., Mikolajewicz, U., Mignot, J., and Biastoch, A.: Decadal fingerprints of freshwater discharge around Greenland in a multi-model ensemble, Climate Dynamics, 41, 695–720, https://doi.org/10.1007/s00382-012-1479-9, 2013.

Taylor, K., Stouffer, R., and Meehl, G.: An overview of CMIP5 and the experimental design, Bulletin of the American Meteorological Society, 93, 485–498, https://doi.org/10.1175/BAMS-D-11-00094.1, 2012.

https://doi.org/10.5194/egusphere-2022-197
Preprint. Discussion started: 4 May 2022

Thompson, A. J., Skinner, C. B., Poulsen, C. J., and Zhu, J.: Modulation of mid-Holocene African rainfall by dust aerosol direct and indirect effects, Geophysical Research Letters, 46, 3917–3926, https://doi.org/10.1029/2018GL081225, 2019.

Tian, B. and Dong, X.: The double-ITCZ bias in CMIP3, CMIP5, and CMIP6 models based on annual mean precipitation, Geophysical Research Letters, 47, https://doi.org/10.1029/2020GL087232, 2020.

Timbal, B. and Arblaster, J. M.: Land cover change as an additional forcing to explain the rainfall decline in the south west of Australia, Geophysical Research Letters, 33, https://doi.org/10.1029/2005GL025361, 2006.

Turner, A. G. and Annamalai, H.: Climate change and the South Asian summer monsoon, Nature Climate Change, 2, 587–595, https://doi.org/10.1038/nclimate1495, 2012.

Valcke, S.: The OASIS3 coupler: A European climate modelling community software, Geoscientific Model Development, 6, 373–388, https://doi.org/10.5194/gmd-6-373-2013, 2013.

Vellinga, M. and Wood, R. A.: Global climatic impacts of a collapse of the Atlantic thermohaline circulation, Climatic change, 54, 251–267, https://doi.org/10.1023/A:1016168827653, 2002.

Vellinga, M. and Wood, R. A.: Impacts of thermohaline circulation shutdown in the twenty-first century, Climatic Change, 91, 43–63, https://doi.org/10.1007/s10584-006-9146-y, 2008.

Wainwright, C. M., Black, E., and Allan, R. P.: Future changes in wet and dry season characteristics in CMIP5 and CMIP6 simulations, Journal of Hydrometeorology, 22, 2339–2357, https://doi.org/10.1175/JHM-D-21-0017.1, 2021.

Wang, B. and Ding, Q.: Global monsoon: Dominant mode of annual variation in the tropics, Dynamics of Atmospheres and Oceans, 44, 165–183, https://doi.org/10.1016/j.dynatmoce.2007.05.002, 2008.

Wang, B., Kim, H.-J., Kikuchi, K., and Kitoh, A.: Diagnostic metrics for evaluation of annual and diurnal cycles, Climate dynamics, 37, 941–955, https://doi.org/10.1007/s00382-010-0877-0, 2011.

Wang, B., Biasutti, M., Byrne, M. P., Castro, C., Chang, C.-P., Cook, K., Fu, R., Grimm, A. M., Ha, K.-J., Hendon, H., et al.: Monsoons climate change assessment, Bulletin of the American Meteorological Society, 102, E1–E19, https://doi.org/10.1175/BAMS-D-19-0335.1, 2021.

Weaver, A. J., Sedláček, J., Eby, M., Alexander, K., Crespin, E., Fichefet, T., Philippon-Berthier, G., Joos, F., Kawamiya, M., Matsumoto, K., et al.: Stability of the Atlantic meridional overturning circulation: A model intercomparison, Geophysical Research Letters, 39, https://doi.org/10.1029/2019JC015083, 2012.

Xin, X., Wu, T., Zhang, J., Yao, J., and Fang, Y.: Comparison of CMIP6 and CMIP5 simulations of precipitation in China and the East Asian summer monsoon, International Journal of Climatology, 40, 6423–6440, https://doi.org/10.1002/joc.6590, 2020.

Zhisheng, A., Guoxiong, W., Jianping, L., Youbin, S., Yimin, L., Weijian, Z., Yanjun, C., Anmin, D., Li, L., Jiangyu, M., et al.: Global monsoon dynamics and climate change, Annual Review of Earth and Planetary Sciences, 43, 29–77, https://doi.org/10.1146/annurev-earth-060313-054623, 2015.

Zhou, T. and Zou, L.: Understanding the predictability of East Asian summer monsoon from the reproduction of land–sea thermal contrast change in AMIP-type simulation, Journal of Climate, 23, 6009–6026, https://doi.org/10.1175/2010JCLI3546.1, 2010.